Biophysical Journal
Article

Biophysical Society

Site-specific water dynamics drives protein stability in hydrated deep eutectic solvents

Tanmoy Khan,[1] Kuntal Debnath,[1] Kuldeep Singh Negi,[1] and Pratik Sen[1,*]
[1]Department of Chemistry, Indian Institute of Technology Kanpur, Kanpur, UP, India

ABSTRACT Deep eutectic solvents (DESs) have gained prominence as promising biocatalytic media owing to their tunability, cost-effectiveness, and biocompatibility. However, a comprehensive mechanistic understanding of protein behavior in such environments remains elusive. In this study, we explore the role of associated water dynamics in modulating the thermal stability of human serum albumin within hydrated choline chloride-glycerol and choline chloride-ethylene glycol DESs. By employing domain-specific site-selective fluorescence labeling and red-edge excitation shift measurement, alongside circular dichroism spectroscopy, we reveal that modulation of associated water dynamics distinctly alters the entropic and enthalpic contributions to the protein stability. Flexible associated water enhances enthalpic stabilization but promotes entropic destabilization, whereas restricted associated water induces the opposite effect, providing a mechanistic basis for the entropy-enthalpy compensation. Our findings underscore the necessity of domain-specific stability measurements in multidomain proteins and highlight the pivotal role of immediate hydration dynamics in protein stabilization within unconventional solvent systems. This study offers valuable insights for the rational design of DES-based biocatalytic systems.

SIGNIFICANCE Understanding protein stability in deep eutectic solvents (DESs) is critical for advancing biocatalysis and biomolecular preservation. This study uncovers how modulation of protein-associated water dynamics governs the thermal stability of proteins in hydrated DESs. Through a combination of domain-specific fluorescence study and thermodynamic analysis, we reveal how associated water flexibility drives entropy-enthalpy compensation at individual domains. Our findings suggest the importance of domain-specific investigations for multidomain proteins. These insights pave the way for designing effective DES-based solvents for enzyme stabilization and biocatalytic applications.

INTRODUCTION

Biocatalysis and deep eutectic solvents

Two key strategies for efficient biocatalysis involve either suitable engineering of the enzyme to keep it stable and active in conventional organic solvents or utilizing tunable solvents that inherently support the native enzyme's stability and activity (1). The first approach, named directed evolution (2–4), was recognized with the 2018 Nobel Prize in chemistry. On the other hand, ionic liquids (ILs) and deep eutectic solvents (DESs), owing to their versatile characteristics, have recently been found to keep enzymes stable and active therein (5–10). Among these two, DES has certain edges over ILs regarding easy, cost-effective, and atom-economical synthesis (9,11,12). Because of all these superior qualities, there has been an upsurge in studies exploring enzymatic behavior in DES and hydrated DES in recent times (6,13–19). However, most reports focus on enzyme stability and activity in DESs without investigating the underlying reasons for enzyme stabilization in these unconventional media.

Theories of enzyme stability in DES

Enzyme stability in DES is often attributed to the network-like structure of DESs, which is primarily formed through extensive hydrogen bonding (15,20,21). Such a structure creates a protective environment that sustains enzyme stability and activity (20,22–24). Additionally, the high viscosity of DESs may restrict enzymes' conformational flexibility, preserving their structural integrity (25–27). Specific hydrogen bonding and ionic interactions between DES components and amino acid residues of an enzyme further influence enzyme conformation and stability (15,20,21). Recently, Fernandez et al. reported that bovine serum albumin and lysozyme can adopt compact globular folds, intermediate states, or unfolded

Submitted May 19, 2025, and accepted for publication October 14, 2025.
*Correspondence: psen@iitk.ac.in
Editor: Guy M. Genin.
https://doi.org/10.1016/j.bpj.2025.10.019

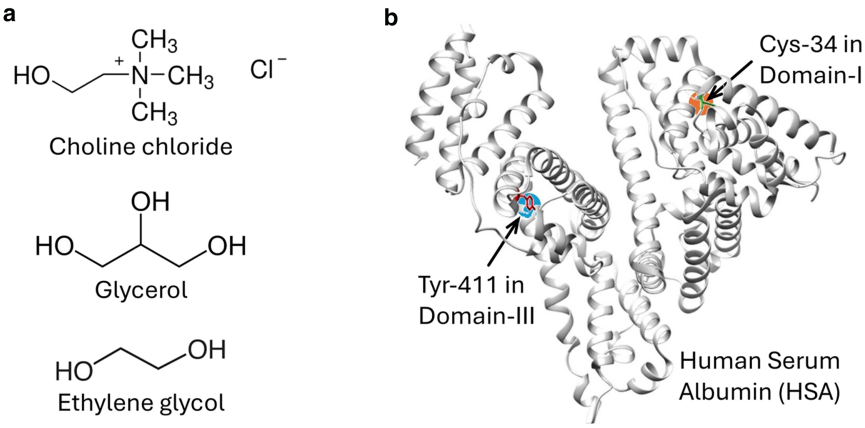

FIGURE 1 Systems of this study. (*a*) The chemical structures of the hydrogen bond acceptor (choline chloride) and donors (glycerol and ethylene glycol) of the used DESs in this study. (*b*) 3D structure of human serum albumin (PDB: 1ha2), where specific sites for domain-specific fluorescence labeling are highlighted.

chains depending on the chemical composition of the DES (28). Few reports even suggest that various physical properties such as polarity, density, refractive index, and surface tension of the DES can also contribute to enzyme thermal stability and catalytic activity (29,30).

Limitations of the current understandings

Although the above understandings are insightful and can explain certain results, they fail to fully account for DES-specific, protein-specific, and DES concentration-dependent stability and activity of enzymes. For instance, lipase, immunoglobulin G, and α-chymotrypsin show higher thermal stability in ChCl-urea DES; yet, lysozyme is destabilized in the same DES (22,31–33). Moreover, in ChCl-urea DES, α-chymotrypsin stabilizes up to 0.25 $g \cdot mL^{-1}$; but its thermal stability decreases at higher DES concentrations (34). Cytochrome C, studied by Papadopoulou et al., exhibits a concentration-dependent activity reversal in several DES, including in ChCl-EG, ChCl-Gly, and ChCl-urea DESs (35). Our group has also reported DES concentration-dependent thermal stability and activity of the enzymes (30,36,37). These observations challenge traditional stability explanations in DES media and indicate the need for a deeper mechanistic understanding.

Role of water dynamics modulation in DES-protein milieu

A closer examination of the literature highlights that hydrated DESs are generally more effective in maintaining enzyme stability and activity compared with anhydrous DESs (15,31,38–40). Multiple studies have shown that even minimal amounts of water can restore enzyme functionality that is otherwise absent in anhydrous DESs (39–41). In fact, several reports further highlight that an optimal level of water is crucial for enhancing enzyme function within DESs (19,42,43). Very recently, Fernandez et al. demonstrated that water modulates enzyme behavior in a nonmonotonic fashion, with optimal hydration levels favoring specific conformations (44). Collectively, these findings emphasize the critical role of water in regulating enzyme behavior in hydrated DES media. Specifically, water in the immediate surroundings that directly interacts with the protein surface, referred to as associated water (which is also known as bound water, biological water, and hydration layer), is known to play a crucial role in maintaining protein stability and activity (45–51). Inspired by these findings, we hypothesize that modulation of associated water dynamics could significantly impact enzyme stability and activity in hydrated DESs (36,37).

Previous studies and their shortcomings

Very recently, we have experimentally shown that less flexible associated water in the presence of hydrated acetamide-urea-sorbitol DES stabilizes an enzyme (bromelain) through the entropic component, but it destabilizes it through the enthalpic component (36). The flexible associated water dynamics influence the thermal stability of bromelain in exactly the opposite way (36). Our hypothesis explained both the positive and negative effects of DES on bromelain (36). However, to generalize this hypothesis, further investigations involving different enzymes and DES compositions are necessary.

Objectives of this study

In this study, we examine human serum albumin (HSA) in the presence of two choline chloride (ChCl)-based DESs, ChCl-glycerol [1:2] (ChCl-Gly) and ChCl-ethylene glycol [1:2] (ChCl-EG), to extend our previous findings on enzyme stability in hydrated DESs. By selecting DESs with different hydrogen bond donors (glycerol vs. ethylene glycol) (Fig. 1), we may be able to determine their specific influence (if any) on enzyme thermal stability. To probe hydration dynamics, we employ a steady-state fluorescence technique

popularly called red-edge excitation shift (REES), which has been used as an indicator of water dynamics (52–55). Given HSA's multidomain structure, site-specific fluorescence labeling allowed us a unique opportunity to examine different domains individually (Fig. 1) (56–58). We have also studied domain-specific thermal stability. Our findings establish a strong correlation between individual entropy and enthalpy contributions to the domain-specific stability and the domain-specific REES, offering insights that could be valuable for biocatalysis in DESs.

MATERIALS AND METHODS

Materials

HSA, 7-diethylamino-3-(4-maleimidophenyl)−4-methylcoumarin (CPM), tetramethylrhodamine-5-maleimide (TMR), ChCl, glycerol, and ethylene glycol were obtained from Sigma-Aldrich (St. Louis, MO) and used as received. Analytical grade di-sodium hydrogen phosphate and sodium dihydrogen phosphate (Merck, India) were used to prepare the buffer (pH 7.4). *p*-Nitrophenyl coumarin ester (NPCE) was synthesized following the previous synthesis procedure reported by our group (57). Dialysis membrane tubing (12-kD cutoff) was from Sigma-Aldrich and activated before use following the procedure given by Sigma-Aldrich, and centrifugal filter units (Amicon Ultra, 10-kD cutoff) were from Merck Millipore, Germany. HPLC-grade dimethyl sulfoxide (DMSO) was from S.D. Fine Chemicals, India.

Protein labeling

CPM and TMR were site-specifically tagged to the only free cysteine-34 group of HSA, and the tyrosine-411 residue was selectively labeled to NPCE using previously reported procedures (37,56,58). We followed almost similar procedure for tagging with all the three dyes. Briefly, 40 mg of HSA was dissolved in 9.8 mL of 50 mM phosphate buffer (pH∼7.4 for CPM and TMR tagging and pH∼8.0 for NPCE tagging), and 0.2 mL of the corresponding dye solution in HPLC grade DMSO was added dropwise with continuous stirring. We have kept the concentration of the dye solution, for CPM and TMR, in such a way that in the final solution, the molar ratio became HSA:dye = 1:1.2. However, for NPCE, HSA:dye = 1:0.87 was kept, avoiding tagging of NPCE at multiple sites (56,59). The reaction mixture was stirred for 12 h at 25°C, followed by dialysis at 5°C using 1000 mL of 15:1 (v/v) phosphate buffer (50 mM (pH 7.4)) and DMSO and changing the dialysis media four times a day for the first 4 days. After that, dialysis was done twice in 24 h with only phosphate buffer till the complete removal of untagged dye (as measured by the absorption and emission spectrum of the dialysis medium). The CPM/TMR/NPCE-tagged HSA was then concentrated using the 10-kDa cutoff centrifugal filtration unit. The tagging efficiency is calculated to be 88%, 75%, and 70% for the CPM-tagged, TMR-tagged, and NPCE-tagged HSA, respectively, from the ratio of the concentration of protein to dye in the CPM/TMR/NPCE-tagged HSA (30). As in many previous reports, we have proved that CPM/TMR/NPCE tagging does not significantly perturb conformation and thermal stability of HSA; we have directly proceeded with the differently labeled HSA for this study (37,56,59).

Preparation of choline chloride-ethylene glycol and choline chloride-glycerol DESs

To prepare the DES, we followed previous reports (34,60,61). Briefly, the constituents were mixed in a sealed container with mole fractions of 0.33 ChCl with 0.66 ethylene glycol or 0.66 glycerol. The mixture was gradually heated to 80°C with continuous stirring. Note that choline chloride was recrystallized in ethanol and dried in a vacuum oven for 12 h before use; ethylene glycol and glycerol were used as received. After 1 hour, a clear DES solution was formed. This DES was stored and used for all experiments, with precautions taken to prevent the incorporation of moisture.

Protein sample preparation

We used 50 mM (pH 7.4) phosphate buffer for all the experiments. HSA samples in experimental media are equilibrated overnight. The concentration of HSA is measured using its molar absorption coefficient of 36,500 $M^{-1}cm^{-1}$ at 280 nm (58). We used untagged HSA for temperature-dependent circular dichroism (CD) spectroscopy measurements, and CPM-tagged and NPCE-tagged HSA were used for both excitation wavelength-dependent and temperature-dependent emission studies. However, for the fluorescence correlation spectroscopy (FCS) study, we have used TMR-tagged HSA because of the availability of a limited LASER facility. HSA concentration was kept at ∼2 μM for the CD spectroscopy, ∼5 nM for the FCS study, and ∼5 μM for the steady-state fluorescence study. In all the cases, the protein is taken from a concentrated aqueous stock, and the concentrations of proteins and the DES in all the hydrated DES samples are maintained by making up the volume with aqueous buffer of pH∼7.4. No experiments were conducted in anhydrous DES.

Circular dichroism spectroscopy

We recorded circular dichroism spectra using a commercial CD spectrometer (J-815, Jasco, Japan) using a 2-mm pathlength cuvette. The temperature was varied from 298 K to 358 K, and the samples were equilibrated for 15 min at each temperature before the measurement. Data were collected in a wavelength range between 190 nm and 260 nm with an integration time of 1 s. Spectra were accumulated over three scans.

Steady-state absorption and emission study

We recorded steady-state absorption and emission spectra using a commercial double-beam spectrophotometer (UV-2450, Shimadzu, Japan) and spectrofluorometer (FluoroMax-4, Jobin-Yvon, USA), respectively, using a 2-mm pathlength cuvette, and the temperature was maintained using an external controller with ±0.5 K precision.

Determination of melting temperature (T_m) from the thermal unfolding curve

The temperature-dependent change CD signal at 222 nm was taken as an indicator of thermal unfolding of HSA in the absence and presence of ChCl-EG and ChCl-Gly DES. For domain-specific unfolding, temperature-dependent fluorescence emission maxima (λ_{ex} = 375 nm for CPM-tagged HSA and λ_{ex} = 435 nm for NPCE-tagged HSA) are used to analyze the thermal unfolding of HSA. The fraction unfolded at each temperature was calculated using Eq. (1) or Eq. (2), depending on the experiment, as in the following (44):

$$f_u = \frac{\theta_{222} - \theta^N_{222}}{\theta^U_{222} - \theta^N_{222}} \text{ (for CD experiment)} \quad (1)$$

or

$$f_u = \frac{\lambda_{max} - \lambda^N_{max}}{\lambda^U_{max} - \lambda^N_{max}} \text{ (for emission experiment)} \quad (2)$$

The fraction unfolded (f_u) parameter, plotted against the temperature, yielded the HSA melting curve at each DES concentration. In the above equation, θ^N_{222} *and* λ^N_{max} represent the CD signal at 222 nm and the emission maximum of the native/folded states of the protein, respectively. Whereas, θ^U_{222} and λ^U_{max} represent the CD signal at 222 nm and the emission maximum of the fully denatured/unfolded states of the protein, respectively. Native/folded and denatured/unfolded states are taken as the lowest and highest values of the CD signal at 222 nm or emission maxima in the thermal denaturation experiment, respectively. The denaturation of protein is considered to be a cooperative phenomenon, and thus, the denaturation pathway follows a sigmoidal nature. Keeping this in mind, here the denaturation plots are fitted with a sigmoidal function given in Eq. (8) (49,51).

$$y = y_N + \frac{y_N - y_U}{1 + e^{\frac{(T_m - T)}{d}}} \tag{3}$$

In the above equation, y_N represents signal corresponding to the native (folded) state of the protein at low temperature, which is taken as 0 (i.e., $f_U = 0$), and y_U represents the signal corresponding to the unfolded state of the protein at high temperature and is taken as 1 (i.e., $f_U = 1$). T_m represents the melting temperature, and d is the slope or cooperativity factor. It describes how sharply the transition occurs. Smaller d values mean a steeper, more cooperative unfolding transition, whereas larger values indicate a broader transition. Note, melting temperature (T_m) is defined as the temperature at which half the protein population is unfolded, i.e., f_u = 0.5, and it indicates the stability of the enzyme.

Thermodynamic analysis of thermal unfolding data

The thermal unfolding of HSA follows a two-state reversible process (62,63) and also from a simple look into the stability curves indicates that a clear two-state model ($N \leftrightarrow U$) can be applied to get the thermodynamic parameters. The equilibrium constant, K_{eq}, for the unfolding of the protein can be written as follows (49,62,64,65):

$$K_{eq} = \frac{f_U}{f_N}, \tag{4}$$

where f_N and f_U are the fraction of protein in the native and unfolded states, respectively. If y_U and y_N are the corresponding emission maxima, then one can represent the emission maxima signal of any point as follows (64):

$$y = y_N f_N + y_U f_U = y_N \frac{1}{1 + K_{eq}} + y_U \frac{K_{eq}}{1 + K_{eq}} \tag{5}$$

Combining Eqs. (4) and (5), we get

$$K_{eq} = \frac{y_N - y}{y - y_u} = \frac{\lambda^N_{max} - \lambda_{max}}{\lambda_{max} - \lambda^U_{max}} \tag{6}$$

Thus, ΔG^0 can be calculated as

$$\Delta G = -RT \ln K_{eq} \tag{7}$$

Also, we know that

$$\Delta G = \Delta H - T\Delta S \tag{8}$$

$$\therefore \Delta G = -RT \ln K_{eq} = \Delta H - T\Delta S \tag{9}$$

The standard enthalpy change (ΔH) and entropy change (ΔS) are determined from the intercept and slope of ΔG versus T plot. Previously, such a model has been used in many reports to yield thermodynamic parameters of HSA (59,62–64). To quantify the effect of DES on the extent of stabilization of HSA, we calculated the differential entropy and enthalpy of unfolding as mentioned in Eqs. (10) and (11).

$$\Delta\Delta H = \Delta H_{DES} - \Delta H_{buffer} \tag{10}$$

$$\Delta\Delta S = \Delta S_{DES} - \Delta S_{buffer} \tag{11}$$

The differential free energy can be defined as

$$\Delta\Delta G = \Delta G_{DES} - \Delta G_{buffer} \tag{12}$$

A positive value of $\Delta\Delta G$ signifies that the system is likely to be in the native state in DES compared with the buffer. As $\Delta\Delta G = \Delta\Delta H$-T$\Delta\Delta S$, a positive value of $\Delta\Delta H$ will be a stabilizing contributor, and a positive value of $\Delta\Delta S$ will be destabilizing.

Fluorescence correlation spectroscopy study

We have performed FCS measurements in a home-built setup. The instrumentation and analysis method can be found in our previous papers and Section S1 of the supporting material (62,64,66,67). Briefly, we measured the diffusion time of TMR-tagged HSA and a standard fluorophore (rhodamine 6G in the present study) in buffer and in different concentrations of two DESs (ChCl-EG and ChCl-Gly) employing FCS. Using this information and the reported value of the diffusion coefficient of rhodamine 6G (R6G) in water (68) ($D_t = 4.14 \times 10^{-6}$ cm^2 s^{-1}) and the hydrodynamic radius of R6G (7.7 Å) in pH 7.4 buffer, the hydrodynamic radius of HSA can be calculated at every experimental point according to the following equation.

$$r_H^{HSA} = r_H^{R6G} \times \frac{\tau_D^{HSA}}{\tau_D^{R6G}} \tag{13}$$

The change in the refractive index is compensated for by changing the objective collar position and setting it to have the highest $G(0)$ and, consequently, the lowest τ_D value for each of the samples. In this way, we maintain the lowest detection volume.

To determine the micro-viscosity, we measured the translational diffusion time (τ_D) of R6G in buffer, DES in water, and in the corresponding constituent aqueous solutions. According to the Stokes-Einstein equation (66), the diffusion coefficient (D_t) is inversely proportional to the viscosity (η) of the medium at a constant temperature. The diffusion coefficient can be related to the inverse of the diffusion times (τ_D) as $D_t \propto 1/\tau_D$. This means, $\tau_D \propto \eta$. Thus, the viscosity of an unknown solution can be obtained from the ratio of diffusion times in the unknown solution and in a reference medium of known viscosity (here, water) as follows (69):

$$\frac{\tau_{D,unknown\ solution}}{\tau_{D,water}} = \frac{Viscosity\ of\ unknow\ solution}{Viscosity\ of\ water} \tag{14}$$

Moreover, as this diffusion occurs at the micron length, it is called micro-viscosity.

RESULTS AND DISCUSSION

Thermal stability of HSA in the presence of choline chloride-based hydrated DES

To investigate the thermal stability of HSA in the presence of hydrated choline chloride-based DESs, choline

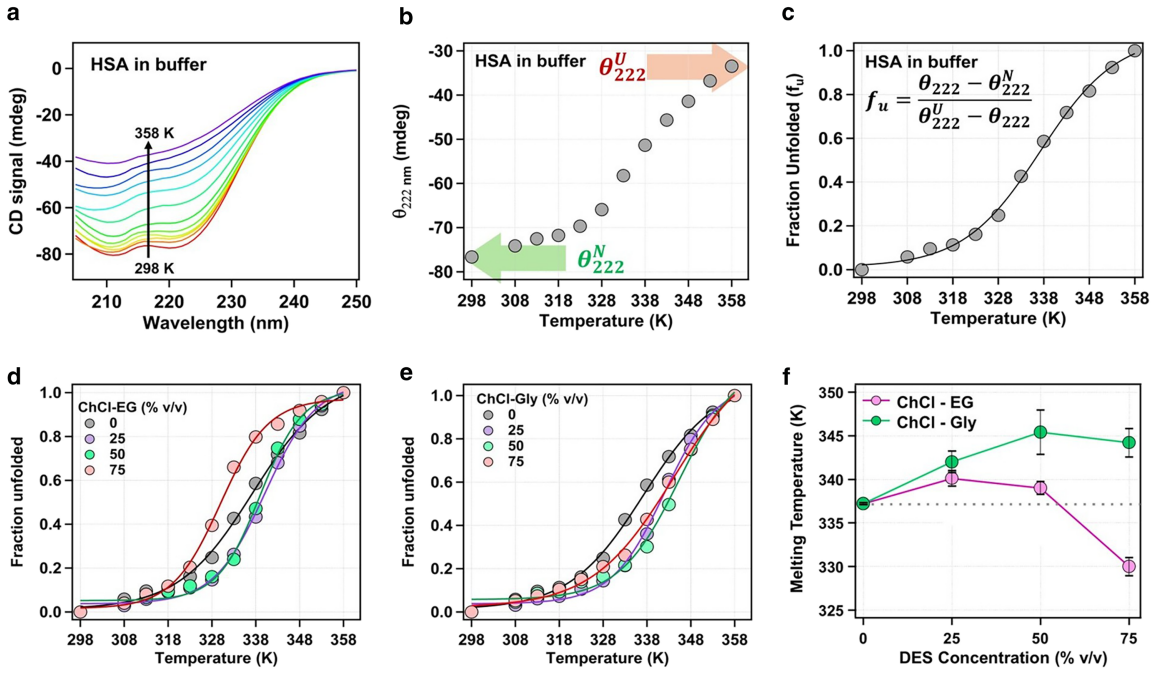

FIGURE 2 Thermal stability of HSA using circular dichroism (CD) spectroscopy. (*a*) Representative CD spectra of HSA in buffer at different temperatures (298–358 K). (*b*) Temperature-dependent change in the CD signal at 222 nm. (*c*) Variation of fraction unfolded (f_u), which has been calculated using the equation mentioned in the inset, as a function of temperature. Comparison of the thermal unfolding curve of HSA in presence of various concentrations of choline chloride-ethylene glycol (ChCl-EG) and choline chloride-glycerol (ChCl-Gly) DESs are shown in (*d*) and (*e*), respectively. Each melting curve was fitted using the sigmoidal function to get the melting temperature of HSA at each DES concentrations. (*f*) Comparison of the melting temperature (T_m) of HSA in the presence of different concentrations of ChCl-EG and ChCl-Gly DESs. The error bar represents the standard deviation of the mean of three independent experiments.

chloride-ethylene glycol [1:2] (ChCl-EG) and choline chloride-glycerol [1:2] (ChCl-Gly), we performed temperature-dependent CD spectroscopic measurements. The CD spectra of HSA in buffer (Fig. 2 *a*) display a clear temperature-dependent shift, with a minima (negative peak) at 222 nm. Temperature-dependent CD spectra of HSA in the presence of different concentrations of the DES are represented in Fig. S2 of the supporting material. Monitoring the CD signal at 222 nm against temperature (Fig. 2 *b*) allowed us to compute the fraction of unfolded protein (f_u) (Fig. 2 *c*) using Eq. (1) and consequently the melting temperature using Eq. (3).

Comparison of the thermal unfolding curves of HSA for varying concentrations of ChCl-EG (Fig. 2 *d*) and ChCl-Gly (Fig. 2 *e*) clearly indicates a nonmonotonic change in the melting temperature (Fig. 2 *f*). Data reveal that at 25% (v/v) DES, the thermal stability of HSA improves in both systems. For higher ChCl-Gly DES concentration, the thermal stability of HSA keeps increasing and tends to saturate. On the other hand, the effect of high concentration of ChCl-EG on HSA is found to be completely opposite, where a destabilization of HSA has been observed (Fig. 2 *f*). Park et al. reported that the enhanced thermal stability of lysozyme in choline chloride-based DES positively correlates with the number of −OH groups in hydrogen bond donors (22). Different DESs with sugars and polyols also showed similar observations for other proteins (29,70–72). Consistent with this trend, a higher stability is observed for ChCl-Gly compared with ChCl-EG. This observation might be attributed, at least in part, to the additional –OH group present in glycerol. Although specific interactions and hydrogen bonding between DES components and protein are typically considered to be the primary stabilizing factors, they fail to explain the concentration-dependent reversal of thermal stability of HSA in ChCl-EG. Moreover, viscosity-driven stabilization cannot account for this trend, as higher DES concentrations (which exhibit increased viscosity) result in reduced protein stability.

Recognition of individual entropic and enthalpic terms of thermal stabilization and entropy-enthalpy compensation

To gain further insights into the thermal stability of HSA in the presence of choline chloride-based DES, we sought to individually recognize the entropy (ΔS) and enthalpy (ΔH) of thermal unfolding at each DES concentration. According to our proposed associated water stabilization mechanism (AWSM) (36,49,62,64), thermodynamic changes in protein systems might be interpreted through the modulation of the dynamics of associated water molecules. Specifically, additive-induced entropic destabilization associated with enthalpic stabilization is expected to result in an increase in the

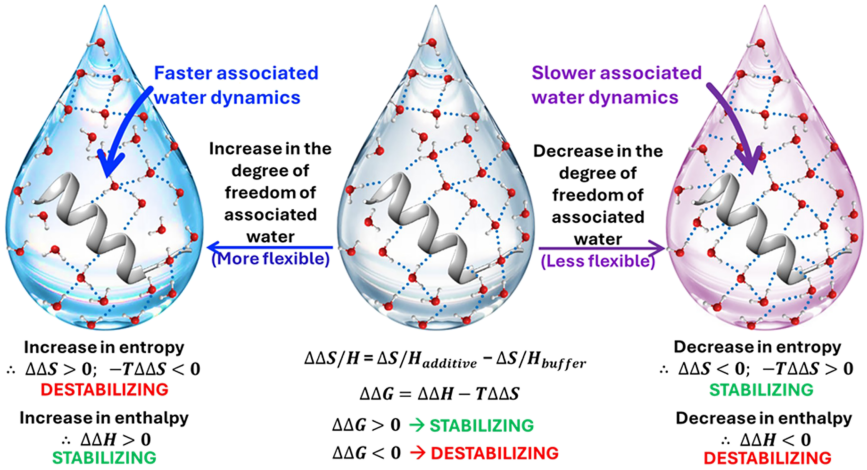

FIGURE 3 Associated water reorganization is a critical factor that modulates protein stability in the presence of additives (here DES). This figure has been represented based on the previous reports from our group (36,49,50).

flexibility of the associated water molecules. In contrast, entropic stabilization and enthalpic destabilization in the presence of additives are predicted to retard the water dynamics (Fig. 3). This relationship can be understood by the modulation of the water-protein hydrogen bond network measured through its dynamics (46). Enhanced flexibility in water dynamics implies a weakened hydrogen bond network, which increases the configurational entropy of water relative to that in the buffer environment. This results in a net positive change in entropy as

$$\Delta\Delta S = \Delta S_{additive} - \Delta S_{buffer} > 0, \quad (15)$$

indicating entropic destabilization of the system. The reduction in hydrogen bond strength requires energy input, typically in the form of heat. This corresponds to a positive enthalpic contribution leading to enthalpic stabilization.

$$Q_P > 0;\ H = Q_P = \left(\frac{dE}{dT}\right)_P dT \quad (16)$$

$$\Delta\Delta H = \Delta H_{additive} - \Delta H_{buffer} > 0 \quad (17)$$

Together, these suggest that associated water dynamics play a critical role in modulating the thermodynamic stability of proteins.

Using the thermal melting curves and a two-state thermodynamic model (Fig. 4 *a*; Section thermodynamic analysis of thermal unfolding data), we have calculated the temperature-dependent free energy of unfolding (ΔG) of HSA across different concentrations of ChCl-EG and ChCl-Gly DES in buffer (Fig. 4 *b* and *c*). By applying the Gibbs-Helmholtz equation, we extracted entropic and enthalpic components of thermal unfolding at each DES concentration. Further, we computed the differential entropy ($\Delta\Delta S$) and enthalpy ($\Delta\Delta H$) of stabilization compared with that in buffer (using Eqs. (10) and (11)) to delineate the positive or negative effect of DES on the protein in an individual entropic and enthalpic manner. The differential free energy of unfolding of the enzyme can be written as

$$\Delta\Delta G = \Delta G_{DES} - \Delta G_{buffer} = \Delta\Delta H - T\Delta\Delta S \quad (18)$$

A positive value of $\Delta\Delta H$ contributes positively to the $\Delta\Delta G$, which implies that DES contributes to the enthalpic stabilization of HSA, whereas a positive value of $\Delta\Delta S$ (consequently, a negative value of $-T\Delta\Delta S$ that contributes negatively to the $\Delta\Delta G$) suggests entropic destabilization. The concentration-dependent differential entropy and enthalpy of stabilization of HSA in the presence of ChCl-EG and ChCl-Gly DESs are presented in Fig. 4 *d* and *e*, respectively. For up to 50% (v/v) of both ChCl-EG and ChCl-Gly DES in buffer, we observed a steady increase in the entropic destabilization and enthalpic stabilization. However, at 75% (v/v) ChCl-EG and ChCl-Gly DES, the extent of both drastically reduces. Further, a plot of $\Delta\Delta H$ versus $-T\Delta\Delta S$ gives a straight line with slope ∼0.85 and 0.83 for ChCl-EG and ChCl-Gly DES, respectively, suggesting a strong entropy-enthalpy compensation in the presence of both the DESs (Fig. 4 *f*). Additionally, the enthalpy effect dominates in the overall stabilization process of HSA in the presence of both DESs.

Entropy-enthalpy compensation is a widely observed phenomenon in biochemical processes (49,50,73,74). In a recent study, we reported a similar compensation effect for bromelain when exposed to acetamide-urea-sorbitol hydrated DES (36). We proposed that water, being a common factor, modulates both entropic and enthalpic contributions in an opposing manner (Fig. 3) (36,49,50). Specifically, we found that less flexible associated water in the presence of DES stabilizes bromelain through entropy but destabilizes it through enthalpy, whereas more flexible associated water result in an opposite thermodynamic outcome (Fig. 3). A similar compensatory effect has been observed in the presence of macromolecular crowders, where modulation of water-protein hydrogen bonds (probed through the associated

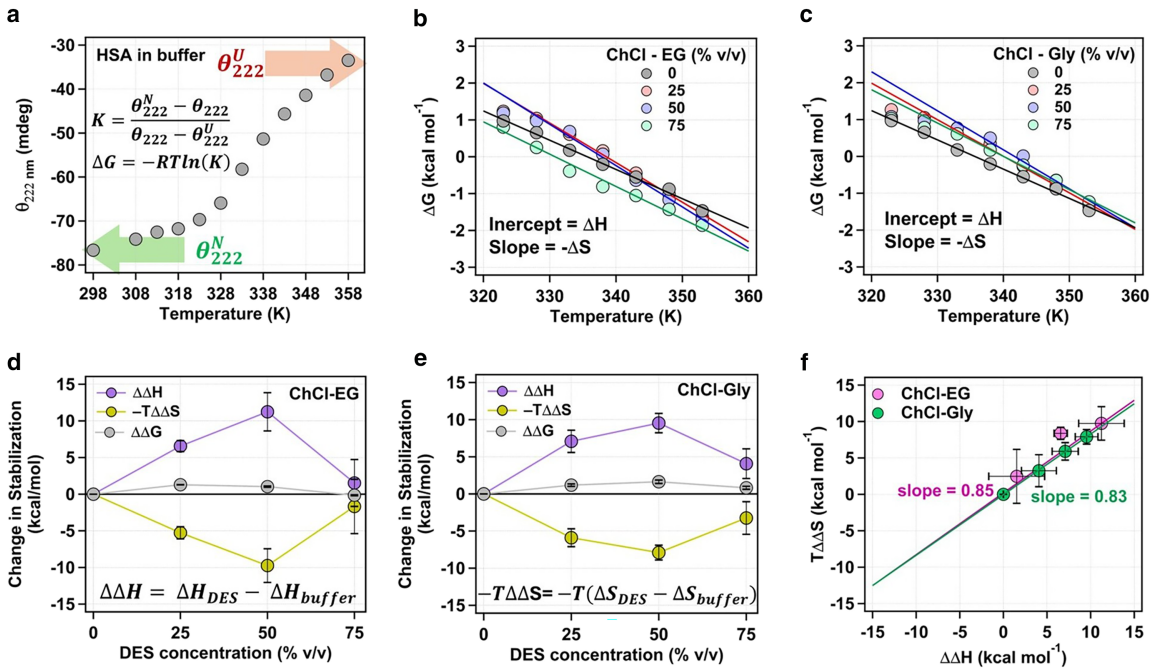

FIGURE 4 Individual entropic and enthalpic components might be positive or negative, depending on the type and concentration of the DES. (*a*) Variation of the CD signal of HSA in buffer at 222 nm with temperature. The equation for calculating the equilibrium constant and the native and denatured state signals is mentioned in the figure. Plot of unfolding free energy of HSA as a function of the temperature in the presence of various concentrations of (*b*) ChCl-EG and (*c*) ChCl-Gly DESs. Plot of differential free energy ($\Delta\Delta G$) at 298 K, differential entropic component ($-T\Delta\Delta S$), and differential enthalpic component ($\Delta\Delta H$) for thermal unfolding of HSA in the presence of various concentrations of (*d*) ChCl-EG and (*e*) ChCl-Gly DESs. Here, $\Delta\Delta H$ *or* $\Delta\Delta G = \Delta H_{DES}$ *or* $\Delta G_{DES} - \Delta H_{buffer}$ *or* ΔG_{buffer}, and $-T\Delta\Delta S = -T(\Delta S_{DES} - \Delta S_{buffer})$, respectively. (*f*) Plot between entropic and enthalpic terms of thermal stability of HSA in the presence of various concentrations of both ChCl-EG (*pink*) and ChCl-Gly (*green*) DESs. The black line is a linear fit, and a near-unity slope indicates entropy-enthalpy compensation. The error bar represents the standard deviation of the mean of three independent experiments.

water dynamics) plays a critical role in protein stability (49,50). Since associated water interacts directly with the protein surface, it likely exerts a significant influence on enzyme stability, and our previous studies support this mechanism (49–51).

To validate the mechanism (i.e., AWSM) further, we aim to investigate solvation dynamics around the protein. We employed steady-state fluorescence-based REES to estimate site-specific solvation dynamics at two different domains of HSA. This approach enables us to generate a residue-specific solvation dynamics map, providing mechanistic insights into the interplay between associated water dynamics and protein stability in DES environments.

Measurement of red-edge excitation shift as an indicator of solvation dynamics

Although NMR and x-ray crystallography can provide insights into the water dynamics, their applicability is limited (75–78). X-ray crystallography primarily reveals only the bound water molecules in the protein crystal (77–79), whereas NMR spectroscopy is generally restricted to small proteins such as calmodulin and lysozyme (80–82). Other advanced techniques, such as Raman and infrared spectroscopy, terahertz spectroscopy, neutron scattering, and dielectric relaxation spectroscopy, offer valuable information on solvation dynamics (83–88). However, these methods are often constrained by complex instrumentation and analysis, intricate sample preparation, and the requirement of high sample concentrations (chances of aggregation), making them less ideal for studying large protein systems (89–92).

In contrast, REES is a fluorescence-based method that is both experimentally simple and highly sensitive to solvation dynamics at site-specific fluorophore locations (52–55,93,94). Unlike other spectroscopic techniques, REES requires only micromolar protein concentrations, making it experimentally accessible for a wide range of biological studies (52,55,56,95). Moreover, high spatial resolution of fluorescence makes REES particularly valuable for investigating solvent interactions in large and complex enzymes (52,55,96,97).

The occurrence of REES depends on the timescale of solvent relaxation relative to the fluorescence lifetime (95,98,99). When the stabilization of the excited state by the surrounding solvent occurs much faster than its fluorescence lifetime ($\tau_S \ll \tau_f$), emission predominantly takes place from the fully solvated state, regardless of the excitation wavelength, and no REES is observed. However, if solvent relaxation is comparable or slower than the excited-state

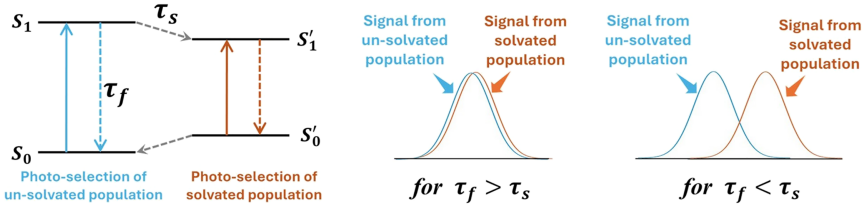

FIGURE 5 Schematic representation of red-edge excitation shift (REES). In a heterogeneous distribution of the environment around the fluorophore, photoexcitation at different wavelengths excites molecules to different excited states (here, S_1 *and* S_1'). When the solvation dynamics (τ_s) is faster than the lifetime (τ_f), irrespective of the excitation wavelength, emission originates from the completely solvent-relaxed state (S_1'), and emission maxima are independent of the excitation wavelength. Consequently, no REES can be observed. When the solvation dynamics is slower than the lifetime, it does not permit the solvent dipolar realignment before the emission, and in this case, the emission originates from a partially solvent-relaxed state for the high-energy excitation and a fully solvent-relaxed state for low-energy excitation. As a result, red-shifted emission spectra and REES can be observed.

lifetime ($\tau_S \geq \tau_f$), emission occurs before complete solvent stabilization, and REES can be observed (Fig. 5) (99).

Since REES only manifests under the conditions of restricted solvent mobility, it serves as a sensitive probe for solvation dynamics around a fluorophore. Additionally, changes in the magnitude of REES in the presence of an additive suggest modulation of solvation dynamics within the system. Specifically, increased REES indicates slower solvation dynamics, revealing critical insights into solvent-protein interactions in diverse environments.

Several reports have proposed that the network-like structure of DES forms a unique solvation shell around the protein, thereby influencing protein stability and dynamics (20,22–24,100). Our group previously demonstrated that even at high concentrations of hydrated acetamide/urea/sorbitol DES, the immediate solvation environment of HSA remains unperturbed (37). Additionally, using bromelain in the same DES system, we experimentally established that modulation of solvation (associated water) dynamics plays a critical role in determining both stability and activity (36). In the present study, we aimed to estimate associated water dynamics through the measurement of REES.

REES has previously been recognized as a reliable indicator of dynamics across diverse protein systems (52,53,56,93,94,96,97,101,102). Raghuraman et al. created a hydration dynamics mapping of K+ channels in their activated and inactivated form employing REES (53). Very recently, More et al. used site-specific REES to develop a solvation dynamics map of TDP-43 protein during misfolding and aggregation (52). The fluorescence lifetime of CPM-tagged HSA (domain-I) and NPCE-tagged HSA (domain-III) in buffer was reported to be around 3.6 ns (56) and 3.7 ns (57), and the solvation time was around 2.2 ns (37) and 1.32 ns (57), respectively. Because of the comparable solvation time and fluorescence lifetime, an appreciable amount of REES has been observed for both domains of HSA. Our group previously reported domain-specific REES changes in HSA during chemical denaturation with guanidine hydrochloride (GnHCl), demonstrating the effect of environmental rigidity on solvent relaxation dynamics (56). Other groups also reported the REES of serum albumin protein (103,104).

Following our previous reports (37,50,56,57), we have selectively tagged two domains of the HSA protein with suitable fluorophores (see Section protein labeling). The excitation wavelength-dependent emission spectra of CPM-tagged HSA (domain-I) and NPCE-tagged HSA in buffer show a clear red shift with the increase in the excitation wavelength (see Fig. 6 *a* and *d*, respectively), and the corresponding excitation wavelength-dependent emission maxima is plotted in Fig. 6 *b* and *e*, respectively, from which the extent of REES is calculated. All the other raw data and relevant plots are incorporated in Sections S3 and S4 of the supporting material.

The extent of REES for CPM tagged to domain-I of HSA is found to increase progressively with an increase in the DES concentration for both ChCl-EG and ChCl-Gly systems (Fig. 6 *c*). In contrast, the REES for NPCE tagged to domain-III of HSA exhibits a nonmonotonic trend (Fig. 6 *f*) in the presence of both ChCl-EG and ChCl-Gly DESs. At low DES concentrations (25% v/v), REES of domain-III decreases, indicating increased flexibility in the nearby water molecules of the protein. At higher DES concentrations (50%–75% v/v), REES increases again, suggesting a restricted solvent environment. The observed domain-specific difference in REES modulation suggests that domain-I experiences progressive solvation retardation, whereas domain-III undergoes an initial increase in the associated water flexibility, followed by somewhat rigidification at higher DES concentrations.

Correlation between entropy and enthalpy of stabilization and associated water dynamics of HSA estimated through REES

To examine the correlation between the associated water dynamics around the protein and its thermal stability, we used $\Delta REES$, defined as

$$\Delta REES = REES_{DES} - REES_{buffer} \quad (19)$$

A positive $\Delta REES$ value indicates retardation of the dynamics near the probe site. Conversely, a negative $\Delta REES$ suggests a more flexible solvent environment, indicating faster associated water dynamics (Fig. 7 *a*). According to the hypothesized AWSM, the entropic stabilization ($\Delta\Delta S<0$ *and* $-T\Delta\Delta S>0$) and concomitant enthalpic

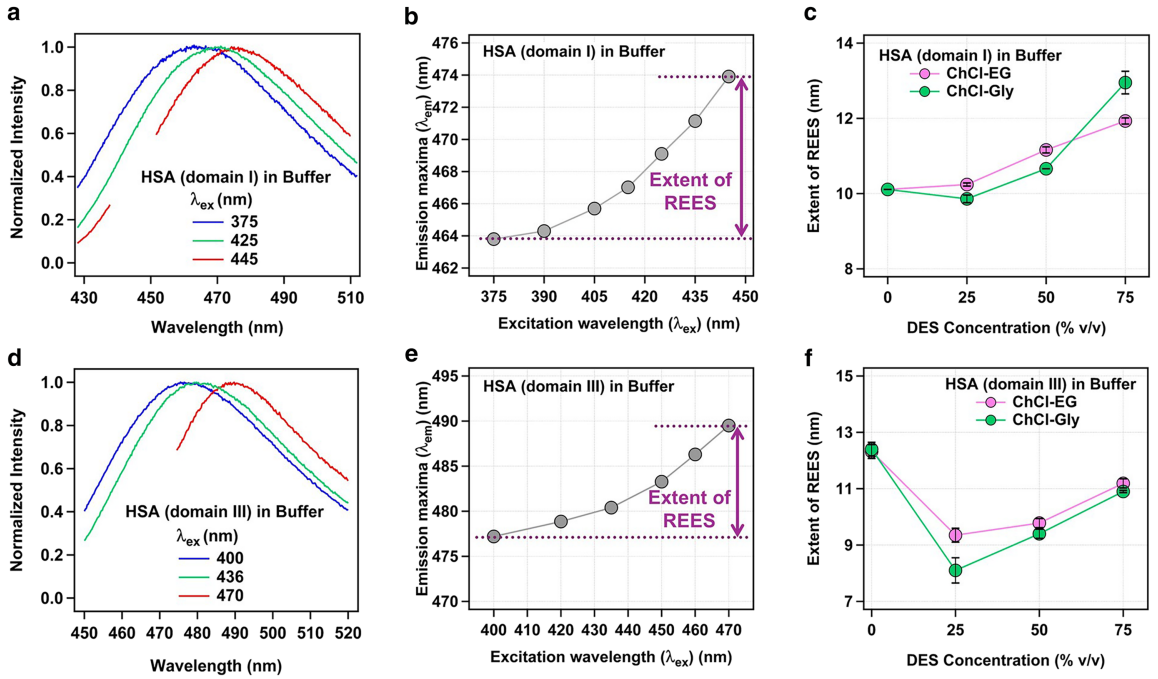

FIGURE 6 Modulation of hydration dynamics employing REES at different domains of HSA. (*a*) Excitation wavelength-dependent emission spectra of CPM tagged to HSA (domain-I) in buffer. (*b*) Shift of the emission maxima of CPM tagged to HSA (domain-I) in the buffer with the change in the excitation wavelength. (*c*) Extent of REES of CPM tagged to HSA (domain-I) in the presence of various concentrations of ChCl-EG (*pink*) and ChCl-Gly (*green*) DES. (*d*) Excitation wavelength-dependent emission spectra of NPCE tagged to HSA (domain-III) in buffer. (*e*) Shift of the emission maxima of NPCE tagged to HSA (domain-III) in the buffer with the change in the excitation wavelength. (*f*) Extent of REES of NPCE tagged to HSA (domain-III) in the presence of various concentrations of ChCl-EG (*pink*) and ChCl-Gly (*green*) DES. The error bar represents the standard deviation of the mean of three independent experiments.

destabilization ($\Delta\Delta H<0$) will be associated with less flexible water dynamics than in buffer, and consequently a positive $\Delta REES$ must be observed (Fig. 7 *b*). On the other hand, the entropic destabilization ($-T\Delta\Delta S<0$) and associated enthalpic stabilization ($\Delta\Delta H>0$) will be linked to the flexible water dynamics than in buffer, and consequently, a negative $\Delta REES$ will be observed (Fig. 7 *b*).

Fig. 4 suggests a negative $\Delta REES$ at low DES concentrations (up to 50% v/v), whereas higher concentrations (75% v/v) of DES should yield less negative or even positive $\Delta REES$. The REES experiment of domain-III of HSA in the presence of both the DESs yields expected results with a negative $\Delta REES$ at low DES concentrations (25%–50% v/v), which become less negative at 75% v/v of DES (Fig. 7 *c* and *f*). In contrast, domain-I of HSA exhibited a different trend. In this case, $\Delta REES$ is found to be positive across all DES concentrations, indicating slower solvation dynamics in the presence of both DESs (Fig. 7 *c* and *f*). Moreover, the magnitude of $\Delta REES$ increased with increasing DES concentration, suggesting a progressive restriction of hydration dynamics in domain-I of HSA. These findings highlight the domain-specific modulation of hydration dynamics in DES environments. Although domain-III experiences an increase in the associated water flexibility for low DES concentrations and then retards with high DES concentrations, domain-I portrays a monotonic retardation of the associated water dynamics.

To further analyze the relationship, we plotted differential entropic and enthalpic changes as a function of $\Delta REES$. Domain-I shows no correlation between $\Delta REES$ and components of thermal stabilization in either ChCl-EG or ChCl-Gly DESs (Fig. 7 *d* and *g*). The negative adjusted R^2 values in Fig. 7 *d* and *g* indicate that $\Delta REES$ of domain-I does not correlate with the overall entropic or enthalpic component of unfolding. However, for domain-III, $\Delta REES$ and differential entropic and enthalpic terms are somehow correlated (Fig. 7 *e* and *h*).

Necessity of domain-specific thermal unfolding of HSA via site-specific fluorescence spectroscopy

The unfolding of multidomain proteins is inherently complex as different domains fold and unfold independently, contributing to the global structure (105–108). Understanding domain-specific unfolding is therefore crucial to elucidate protein stabilization mechanisms (109–111). HSA consists of three distinguishable domains (112). Among these, REESs of domain-I and -III are probed in the present study through selective fluorescent tags. Fortunately, through these domain-selective fluorescent tags, domain-specific thermal unfolding can also be measured.

Our previous research demonstrated that domain-III of HSA unfolds first, followed by domain-I and -II,

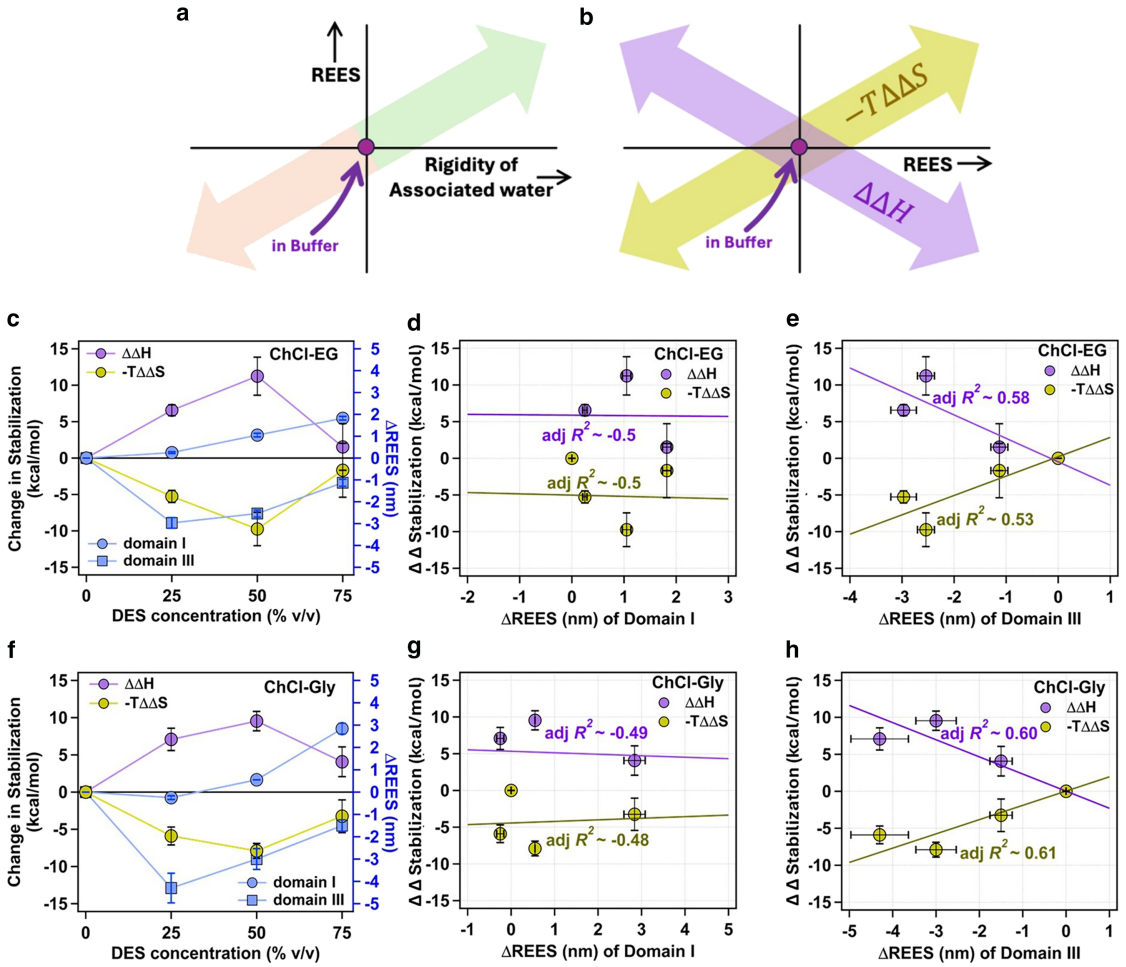

FIGURE 7 Correlation between the overall thermal stability of HSA and modulation of REES of two different domains of HSA. (*a*) Schematic representation of the relation between *REES* and the modulation of solvation/hydration dynamics with respect to the buffer. (*b*) A schematic representation of our hypothesis, where entropic stabilization and associated enthalpic destabilization suggest slower hydration dynamics than in buffer (more *REES* than buffer, i.e., positive $\Delta REES$), and the opposite thermodynamic outcome, which is entropic destabilization and associated enthalpic stabilization, suggests faster hydration dynamics, i.e., negative $\Delta REES$. (*c*) Differential entropic component ($-T\Delta\Delta S$) and enthalpic component ($\Delta\Delta H$) of thermal unfolding of HSA and the differential REES ($\Delta REES = REES_{DES}$ - $REES_{buffer}$) of domain-I and domain-III in the presence of various concentrations of ChCl-EG. Plot of differential stability components ($\Delta\Delta H$ and $-T\Delta\Delta S$) of thermal unfolding of HSA in the presence of various concentrations of ChCl-EG DES as a function of the $\Delta REES$ of (*d*) domain-I and (*e*) domain-III. (*f*) Differential entropic component ($-T\Delta\Delta S$) and enthalpic component ($\Delta\Delta H$) of thermal unfolding of HSA and the differential REES ($\Delta REES$) of domain-I and domain-III in the presence of various concentrations of ChCl-Gly DES. Plot of differential stability components ($\Delta\Delta H$ and $-T\Delta\Delta S$) of thermal unfolding of HSA in the presence of various concentrations of ChCl-Gly DES as a function of the $\Delta REES$ of (*g*) domain-I and (*h*) domain-III. No correlation was found in the case of $\Delta REES$ of domain-I for both the DESs. The error bar represents the standard deviation of the mean of three independent experiments.

when exposed to guanidine hydrochloride (GnHCl) (109–111,113,114). Mohan et al. even reported the domain-specific solvation dynamics of HSA in the presence and absence of sucrose during unfolding, revealing different modulation of the hydration dynamics across domains (115). Other studies have explored domain-specific secondary structure and binding properties of HSA (112). Inspired by these studies, we aimed to measure domain-specific stabilization of HSA in the presence of ChCl-EG and ChCl-Gly DESs.

Thermal unfolding of domain-I of HSA is monitored through the change in the emission characteristics of CPM dye tagged to domain-I of HSA. CPM is a solvatochromic dye having high sensitivity to its microenvironment. In native HSA, CPM is buried within hydrophobic regions of domain-I, leading to a blue-shifted emission. However, upon protein unfolding, CPM becomes exposed to aqueous surroundings, causing a red-shifted emission (Fig. 8 *a* and *b*) as its excited-state dipole gets stabilized through the polar solvent (water) relaxation (116). This environment-dependent spectral shift makes CPM fluorescence a sensitive indicator of protein unfolding. All the other relevant raw data and thermal unfolding curves are represented in Section S5 of the supporting material.

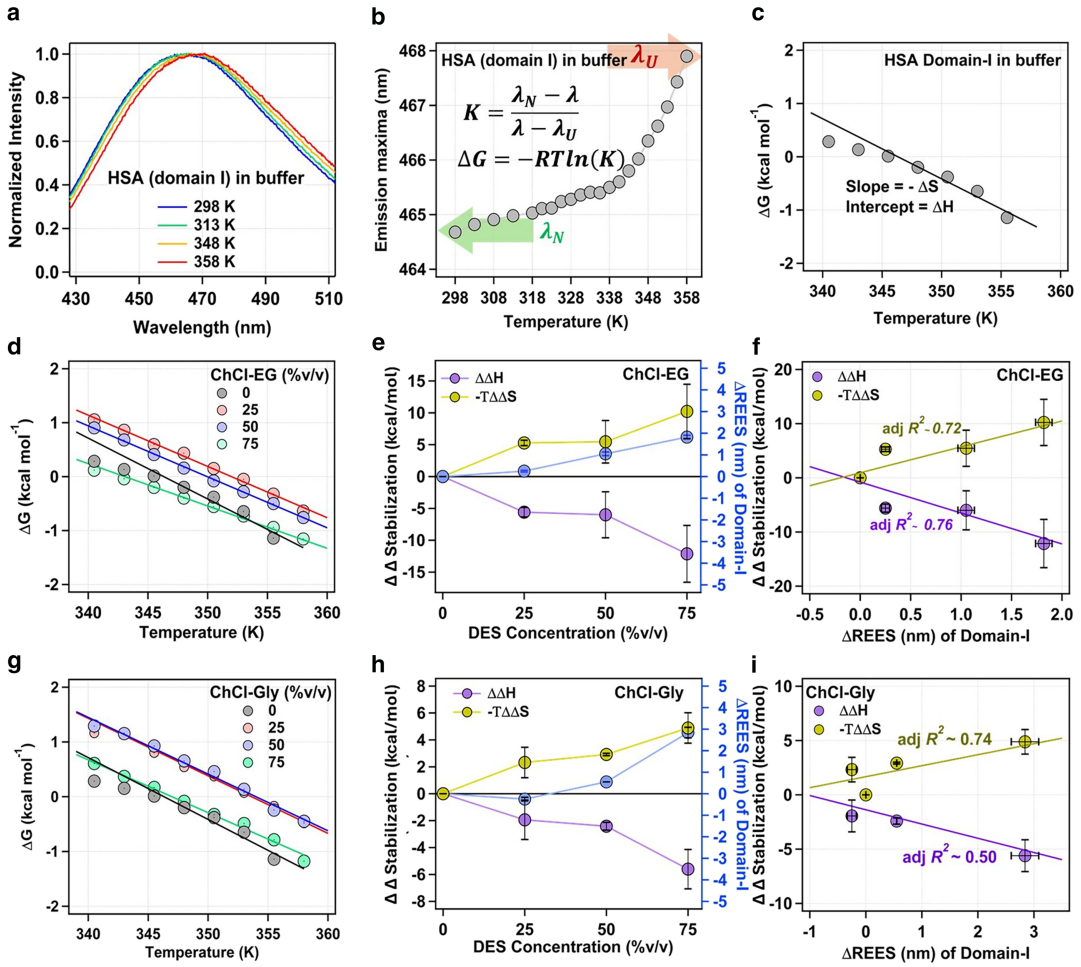

FIGURE 8 Thermal unfolding of domain-I of HSA and its correlation with modulation of REES of domain-I in the presence of different DESs. (*a*) Representative steady-state fluorescence spectra of CPM-tagged HSA (domain-I) in buffer at different temperatures. (*b*) Variation of emission maxima of CPM-tagged HSA in buffer as a function of temperature. (*c*) Schematic for estimating the change in the entropy and the enthalpy from the slope and the intercept, respectively, from the unfolding free energy of domain-I of HSA in buffer. Plot of unfolding free energy of domain-I of HSA in the presence of various concentrations of (*d*) ChCl-EG and (*g*) ChCl-Gly DESs as a function of the temperature. Differential entropic component ($-T\Delta\Delta S$) and enthalpic component ($\Delta\Delta H$) of thermal unfolding of domain-I of HSA and the differential REES ($\Delta REES = REES_{DES}$ - $REES_{buffer}$) of domain-I in the presence of various concentrations of (*e*) ChCl-EG and (*h*) ChCl-Gly DESs. Plot of differential stability components ($\Delta\Delta H$ and $-T\Delta\Delta S$) of thermal unfolding of HSA as a function of the $\Delta REES$ of domain-I in the presence of various concentrations of (*f*) ChCl-EG and (*i*) ChCl-Gly DESs. The error bar represents the standard deviation of the mean of three independent experiments.

From the thermal unfolding curve of domain-I of HSA in the absence and presence of different concentrations of the two DESs, we determined the free energy of the unfolding employing a two-state model (Eq. (1)). Using the Gibbs-Helmholtz equation, we recognized the individual entropic and enthalpic terms of the thermal unfolding (see Fig. 8 *c* for buffer; Fig. 8 *d* for varying concentrations of ChCl-EG; Fig. 8 *g* for varying concentrations of ChCl-Gly). We then calculated the differential entropy and enthalpy of thermal unfolding, taking the entropy and enthalpy of unfolding in buffer as a baseline. In Fig. 8 *e* and *h*, we have plotted differential entropy and enthalpy of domain-I unfolding alongside $\Delta REES$, across different concentrations of ChCl-EG and ChCl-Gly DESs, respectively. Clearly, with the entropic stabilization ($-T\Delta\Delta S>0$) and concomitant enthalpic destabilization ($\Delta\Delta H<0$), a positive $\Delta REES$ is observed, which suggests a retarded associated water dynamics. Moreover, the highest DES concentrations yielded the strongest positive $\Delta REES$, reinforcing the hypothesis that restriction in the associated water contributes to thermal stabilization. Consequently, a very strong correlation between differential entropy and enthalpy with $\Delta REES$ has been observed in the case of both the DESs (Fig. 8 *f* and *i*), which was previously absent when correlated with the entropy and enthalpic components of overall stabilization (Fig. 7 *d* and *g*).

To explore the stabilization of domain-III of HSA, we used the solvatochromic feature of NPCE tagged to domain-III of HSA. The temperature-dependent emission spectra and the shift of emission maxima of NPCE-tagged HSA in buffer are represented in Fig. 9 *a* and *b*, respectively.

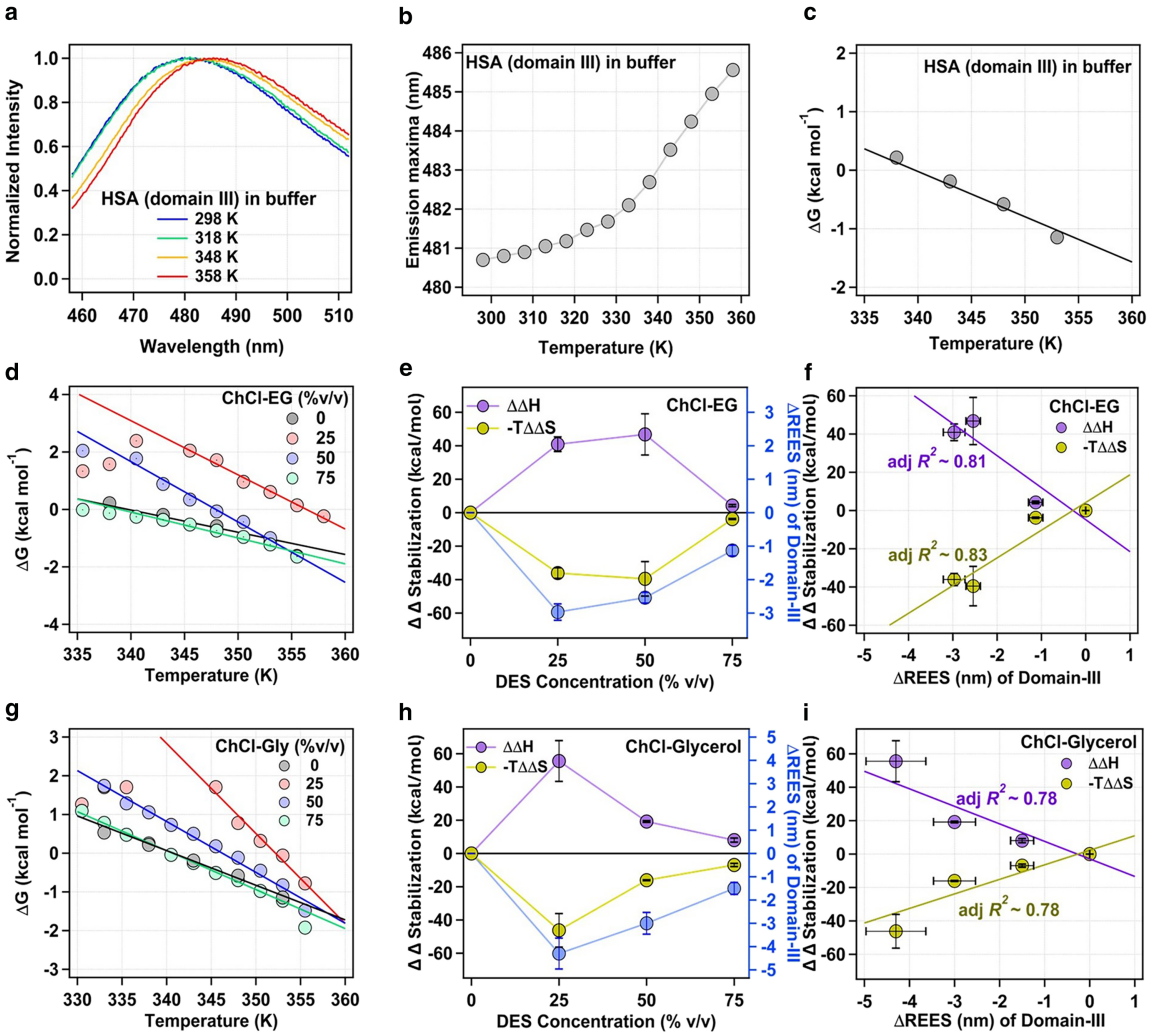

FIGURE 9 Thermal unfolding of domain-III of HSA and its correlation with modulation of REES of domain-III in the presence of different DESs. (*a*) Representative steady-state fluorescence spectra of NPCE-tagged HSA (domain-III) in buffer at different temperatures. (*b*) Variation of emission maxima of NPCE-tagged HSA in buffer as a function of temperature. (*c*) Schematic for estimating the change in the entropy and the enthalpy from the slope and the intercept, respectively, from the unfolding free energy of domain-III of HSA in buffer. Plot of unfolding free energy of domain-III of HSA in the presence of various concentrations of (*d*) ChCl-EG and (*g*) ChCl-Gly DESs as a function of the temperature. Differential entropic component ($-T\Delta\Delta S$) and enthalpic component ($\Delta\Delta H$) of thermal unfolding of domain-III of HSA and the differential REES ($\Delta REES = REES_{DES}$ - $REES_{buffer}$) of domain-III in the presence of various concentrations of (*e*) ChCl-EG and (*h*) ChCl-Gly DESs. Plot of differential stability components ($\Delta\Delta H$ and $-T\Delta\Delta S$) of thermal unfolding of HSA as a function of the $\Delta REES$ of domain-III in the presence of various concentrations of (*f*) ChCl-EG and (*i*) ChCl-Gly DESs. The error bar represents the standard deviation of the mean of three independent experiments.

The unfolding data in the presence of different concentrations of ChCl-EG and ChCl-Gly DESs are presented in Section S5 of the supporting material. Employing the Gibbs-Helmholtz equation (Eq. (8)) in the free energy of unfolding versus temperature plots, we have extracted the entropy and enthalpy of unfolding in buffer and at each experimental concentration of the two DESs (Fig. 9 *c*, *d*, and *g*). In Fig. 9 *e* and *h*, we have plotted differential entropy and enthalpy of domain-III unfolding along with the $\Delta REES$ of that domain, in the presence of different concentrations of ChCl-EG and ChCl-Gly DES, respectively. Negative $\Delta REES$ is consistently observed across all DES concentrations, confirming that associated water dynamics around domain-III become more flexible in DES environments. Also, the differential entropy and enthalpy are well correlated as a function of $\Delta REES$ (Fig. 9 *f* and *i*) and the adjusted R^2, which indicates that the goodness of fit substantially increases. These findings reinforce the hypothesis that associated water dynamics significantly influence protein thermal stability, consistent with prior observations in other DESs and macromolecular crowders (36,49–51). Moreover, these observations suggest a need for domain-specific measurement of thermal unfolding and solvation dynamics in the case of multidomain proteins.

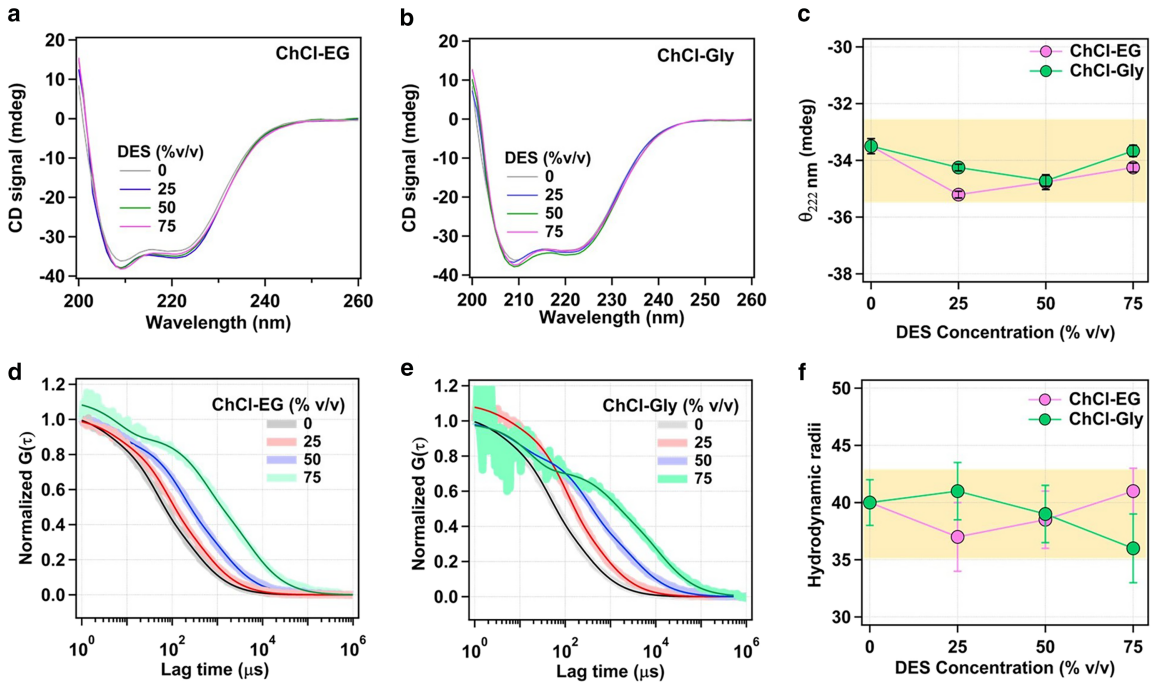

FIGURE 10 No significant conformational change of HSA in the presence of both ChCl-based DESs. CD spectra of HSA at different concentrations of (*a*) ChCl-EG and (*b*) ChCl-Gly hydrated DESs. (*c*) experimental intensity of CD spectra at 222 nm at each DES concentration, which shows that the secondary structure is not significantly perturbed throughout the concentration range of DES. The normalized correlation function obtained using FCS for TMR-tagged (domain-I) of HSA in the presence of different concentrations of (*d*) ChCl-EG and (*e*) ChCl-Gly hydrated DESs. *Solid lines* represent fitting with the equation. S3. (*f*) Modulation of hydrodynamic radii of HSA with the concentrations of hydrated DES. The error bar represents the standard deviation of the mean of three independent experiments.

Role of protein conformation in modulating the REES of HSA

Thus far, we have demonstrated a correlation between individual entropic and enthalpic terms of the domain-wise stability of HSA and the modulation of associated water dynamics around that domain probed through REES. However, changes in the protein conformations due to the addition of DES can also influence the thermal stability and the associated water dynamics. Also, if the protein conformations change significantly due to the DES addition, it might affect the extent of REES as well. Protein unfolding generally leads to increased water interaction that accelerates the associated water dynamics (110,113,115). Our group previously reported that increasing GnHCl concentrations resulted in the unfolding of domain-I and domain-III of HSA with a significant decrease in the extent of REES (56). Thus, one needs to be assured of the minimal structural changes of the protein in the presence of different hydrated DESs to comment on any relationship present between stability and REES and, consequently, associated water dynamics.

To examine whether DES affects the secondary structure of HSA, we performed CD spectroscopy at different DES concentrations. No significant spectral changes were observed with increasing ChCl-EG or ChCl-Gly DES concentrations, indicating no substantial alterations in protein conformation (Fig. 10 *a–c*). To further assess any DES-induced global tertiary structural changes, we used single-molecule-level FCS to determine the hydrodynamic radii of HSA in the presence of different concentrations of both the hydrated DESs (see Fig. 10 *d–f*; Section fluorescence correlation spectroscopy study for details). We found no significant change in the hydrodynamic radii in the presence of ChCl-EG. However, a slight compaction in the structure (decrease in the hydrodynamic radius) at 75% (v/v) of ChCl-Gly hydrated DES (Fig. 10 *f*) is observed. These results collectively confirm that structural changes do not play a significant role in DES-mediated domain-specific stabilization of HSA and further validate associated water dynamics modulation as the key factor influencing protein stability in DES media.

Structural nature of DES-water mixtures and role of individual components

The persistence of the hydrogen-bonded network in DES-water mixtures has been a subject of considerable debate in the DES research community (117–120). Literature reports suggest that beyond a certain threshold of water, the system increasingly resembles an aqueous solution of the individual components of the DES. For example, Hammond et al. reported that the DES network of ChCl-urea system is retained

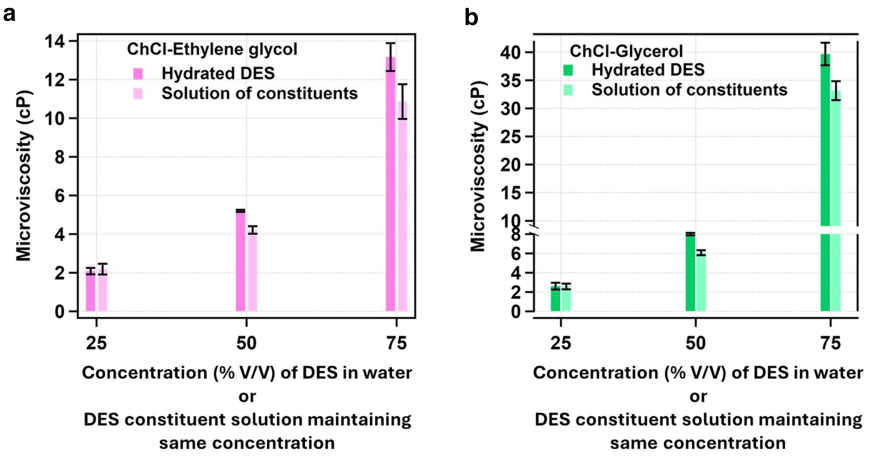

FIGURE 11 Comparison of micro-viscosity of the hydrated DES (*dark shade*) and the aqueous solution of DES constituents of the same concentration as in hydrated DES (*light shade*) for (*a*) choline chloride-ethylene glycol DES and (*b*) choline chloride-glycerol DES systems. The error bar represents the standard deviation of the mean of three independent experiments.

up to ∼42% (W/W) of water (119). Using NMR, Ferreira et al. found that the nanostructure of ChCl-glycerol DES remains intact up to ∼35% (W/W) water (118). Through density, refractive index, and thermal expansion coefficient measurements along with DFT study, Rozas et al. demonstrated that for ChCl-ethylene glycol DES, the fundamental features of the eutectic structure are maintained up to ∼30% (W/W) water (117). Using reported densities (61), these thresholds correspond to ∼68% (V/V) ChCl-glycerol DES in water and ∼72% (V/V) ChCl-ethylene glycol DES in water. Therefore, the 75% (V/V) DES compositions in the present study are very much within the above limit, where DES-specific structuring is largely maintained.

To further probe whether such structuring persists in our systems, we compared the micro-viscosity estimated from the translational diffusion of rhodamine 6G in hydrated DESs and in aqueous solutions of DES constituents of the same concentration as in hydrated DES using FCS. Previously, for hydrated acetamide-urea-sorbitol DES, our group has shown that from 30% (V/V) DES in water, the micro-viscosity of hydrated DES differs appreciably from the micro-viscosity of the aqueous solution of DES constituents of the same concentration as in hydrated DES, which suggests the existence of a network-like DES structure at such concentrations (37). For the present case, the estimated micro-viscosities of hydrated DESs and those of the aqueous solution of DES constituents of the same concentration as in hydrated DES are depicted in Fig. 11 (see Section S6 of the supporting material for relevant data). It is evident that for 50% (V/V) and above DES in water, the micro-viscosities of hydrated DESs are more compared with those in the aqueous solution of DES constituents of the same concentration as in hydrated DES, suggesting the retention of DES-specific hydrogen-bonded structure, which cannot be reproduced by simply mixing the components in water.

We next examined whether individual DES constituents contribute similarly to protein stability and water dynamics as in the case of DESs. Thermal stability (Fig. 12 *a*) was measured for HSA in the presence of choline chloride, ethylene glycol, and glycerol individually at concentrations matching those in the hydrated DESs. All the relevant raw data and the melting curves can be found in Section S7 of the supporting material. Ethylene glycol had a negligible impact on T_m at all concentrations tested, whereas choline chloride produced a small but concentration-independent increase in the T_m. On the other hand, glycerol induced a modest concentration-dependent change in the T_m value. Nevertheless, these effects of the individual components are minor and do not approach the magnitude or trend of stability observed in hydrated DES. REES measurements (see Sections S8 and S9 of the supporting material) for both domains I and III (Fig. 12 *b*) likewise showed negligible changes for all component solutions, in sharp contrast to hydrated DESs (Fig. 6 *c* and *f*).

Together, these results demonstrate that the effects observed in hydrated DESs are not simply the sum of individual component contributions. Rather, they arise from a synergistic interplay between DES constituents and the preserved DES network, which collectively modulate protein-associated water dynamics and stability. Although molecular-level quantification of hydrogen-bonding interactions (e.g., MD simulation or NMR study) would provide additional mechanistic detail, such studies are beyond the scope of the present work and are planned for future investigations. Moreover, we want to emphasize that the persistence of a bulk DES network is not the central focus of the present work. Our mechanistic conclusions are based on the correlation between protein-associated water dynamics (measured via REES) and thermal stability, which is unrelated to the intact hydrogen-bonded network of the DES-water system at the bulk scale.

CONCLUSION

This study elucidates the critical role of hydration dynamics in modulating protein stability within hydrated DESs, using

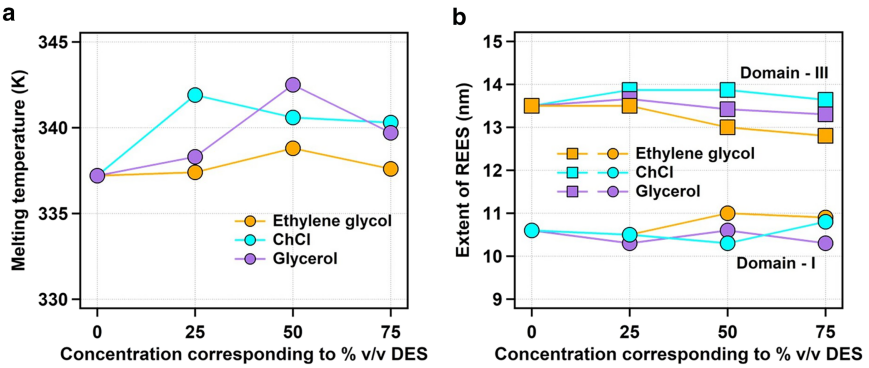

FIGURE 12 Stability and hydration dynamics of HSA in the solution of individual constituents. (*a*) Comparison of the melting temperature (T_m) of HSA in the presence of different concentrations of ethylene glycol, choline chloride, and glycerol corresponding to the respective hydrated DES. (*b*) Extent of REES of CPM tagged to HSA (*circle*) and NPCE tagged to HSA (*square*) in the presence of various concentrations of ethylene glycol, choline chloride, and glycerol corresponding to the respective hydrated DES solution.

HSA as a model system. By employing CD spectroscopy, fluorescence-based REES, and fluorescence spectroscopy, we systematically investigated the interplay between solvation dynamics, entropy-enthalpy compensation, and protein stability in the presence of choline chloride-based hydrated DESs (ChCl-EG and ChCl-Gly).

Our findings reveal that, firstly, hydration dynamics can be measured through a simple fluorescence-based technique, REES. More importantly, hydration dynamics rather than protein conformational changes dictate the thermal stability of HSA in choline chloride-based hydrated DESs.

Secondly, domain-specific unfolding is an important measurement to understand the intricate relationship between enzyme stability and hydration dynamics. Strong correlations between hydration dynamics ($\Delta REES$) and stability components ($-T\Delta\Delta S$ and $\Delta\Delta H$) affirm hydration-induced protein stabilization in DESs. Domain-specific REES changes directly correlate with stability trends, reinforcing the mechanistic link between hydration dynamics and entropy-enthalpy compensation.

Thirdly, domain-specific hydration modulation probably governs the entropy-enthalpy balance of protein stabilization. Domain-I exhibits retarded associated water dynamics (positive $\Delta REES$), leading to enthalpic destabilization and entropic stabilization, whereas domain-III experiences hydration flexibility (negative $\Delta REES$), resulting in enthalpic stabilization and entropic destabilization.

Fourthly, ChCl-Gly DES exerts a stronger stabilizing effect than ChCl-EG, which might be attributed, at least in part, to differences in hydrogen bond donor interactions arising from the higher number of –OH groups in glycerol compared with ethylene glycol.

Fifthly, by comparing the thermal stability and REES of HSA in the presence of individual DES components, this study shows that the effects observed in hydrated DESs do not arise from the components in isolation, but from a synergistic interplay of constituents together with the DES-like network structure, which critically modulates associated water dynamics and protein stability.

Overall, our results provide a fundamental understanding of protein-DES interactions by identifying hydration dynamics (associated water dynamics) as a key determinant of protein stability. Although this work focuses on HSA in DES-water mixtures, previous studies from our group have validated AWSM across different proteins (e.g., bromelain) and additives (DES, crowders). This suggests that AWSM represents a general framework for understanding how modulation of associated water dynamics influences protein stability. Future work should extend these analyses to enzymes with active sites that are highly sensitive to solvent-induced hydration changes, enabling prediction and design of DES compositions tailored for both stability and catalytic performance.

ACKNOWLEDGMENTS

T.K. thanks the Prime Minister Research Fellowship, Government of India, for graduate studies. K.D. and K.S.N. gratefully acknowledge the University Grants Commission (UGC), Government of India, and IIT Kanpur, respectively, for providing a graduate fellowship. P.S. thanks the Indian Institute of Technology Kanpur for infrastructure and the Poonam and Prabhu Goel Chair position of IIT Kanpur for support. Authors acknowledge Ms. Bindu Yadav and Prof. P. Venkatesu of University of Delhi, India for help in CD measurements. This work is financially supported by the Science and Engineering Research Board, Government of India (grant no. CRG/2022/002324).

AUTHOR CONTRIBUTIONS

T.K., conceptualization, visualization, methodology, investigation, formal analysis, data curation, writing original draft, and review & editing. K.D., data curation, formal analysis, discussion, and writing original draft. K.S.N., discussion and review & editing. P.S., conceptualization, visualization, discussion, review & editing, supervision, and funding acquisition.

DECLARATION OF INTERESTS

The authors have no conflicts of interest to declare.

SUPPORTING MATERIAL

Supporting material can be found online at https://doi.org/10.1016/j.bpj.2025.10.019.

REFERENCES

1. Stepankova, V., S. Bidmanova, …, J. Damborsky. 2013. Strategies for stabilization of enzymes in organic solvents. *ACS Catal.* 3:2823–2836.
2. Arnold, F. H. 2018. Directed Evolution: Bringing New Chemistry to Life. *Angew. Chem. Int. Ed.* 57:4143–4148.
3. Krämer, K. 2018. What is directed evolution and why did it win the chemistry Nobel prize? | News. *Chem. World*. https://www.chemistryworld.com/news/what-is-directed-evolution-and-why-did-it-win-the-chemistry-nobel-prize/3009584.article.
4. Kan, S. B. J., R. D. Lewis, …, F. H. Arnold. 2016. Directed evolution of cytochrome c for carbon-silicon bond formation: Bringing silicon to life. *Science.* 354:1048–1051.
5. van Rantwijk, F., and R. A. Sheldon. 2007. Biocatalysis in ionic liquids. *Chem. Rev.* 107:2757–2785.
6. Pätzold, M., S. Siebenhaller, …, D. Holtmann. 2019. Deep Eutectic Solvents as Efficient Solvents in Biocatalysis. *Trends Biotechnol.* 37:943–959.
7. Sheldon, R. A. 2021. Biocatalysis in ionic liquids: State-of-the-union. *Green Chem.* 23:8406–8427.
8. Florindo, C., F. Lima, …, I. M. Marrucho. 2019. Deep eutectic solvents: overcoming 21st century challenges. *Curr. Opin. Green Sustainable Chem.* 18:31–36.
9. Smith, E. L., A. P. Abbott, and K. S. Ryder. 2014. Deep Eutectic Solvents (DESs) and Their Applications. *Chem. Rev.* 114:11060–11082.
10. Paiva, A., R. Craveiro, …, A. R. C. Duarte. 2014. Natural deep eutectic solvents - Solvents for the 21st century. *ACS Sustain. Chem. Eng.* 2:1063–1071.
11. Płotka-Wasylka, J., M. de la Guardia, …, M. Vilková. 2020. Deep eutectic solvents vs ionic liquids: Similarities and differences. *Microchem. J.* 159:105539.
12. Domínguez de María, P., and Z. Maugeri. 2011. Ionic liquids in biotransformations: From proof-of-concept to emerging deep-eutectic-solvents. *Curr. Opin. Chem. Biol.* 15:220–225.
13. Yadav, N., and P. Venkatesu. 2022. Current understanding and insights towards protein stabilization and activation in deep eutectic solvents as sustainable solvent media. *Phys. Chem. Chem. Phys.* 24:13474–13509.
14. Kist, J. A., H. Zhao, …, G. A. Baker. 2021. The study and application of biomolecules in deep eutectic solvents. *J. Mater. Chem. B.* 9:536–566.
15. Juneidi, I., M. Hayyan, …, A. Hayyan. 2017. Pure and aqueous deep eutectic solvents for a lipase-catalysed hydrolysis reaction. *Biochem. Eng. J.* 117:129–138.
16. Sanchez-Fernandez, A., and A. J. Jackson. 2021. Proteins in deep eutectic solvents: Structure, dynamics and interactions with the solvent. *In* Advances in Botanical Research. R. Verpoorte, G.-J. Witkamp, and Y. H. Choi, eds Academic Press Inc, pp. 69–94.
17. Toledo, M. L., M. M. Pereira, …, A. P. M. Tavares. 2019. Laccase Activation in Deep Eutectic Solvents. *ACS Sustain. Chem. Eng.* 7:11806–11814.
18. Huang, Z. L., B. P. Wu, …, Z. Yang. 2014. Deep eutectic solvents can be viable enzyme activators and stabilizers. *J. Chem. Technol. Biotechnol.* 89:1975–1981.
19. Tian, Y., M. Zhu, …, C. Liu. 2023. Natural deep eutectic solvent—A novel green solvent for protein stabilization. *Int. J. Biol. Macromol.* 247:125477.
20. Monhemi, H., M. R. Housaindokht, …, M. R. Bozorgmehr. 2014. How a protein can remain stable in a solvent with high content of urea: Insights from molecular dynamics simulation of Candida antarctica lipase B in urea: Choline chloride deep eutectic solvent. *Phys. Chem. Chem. Phys.* 16:14882–14893.
21. Zeng, C. X., S. J. Qi, …, Y. H. Wang. 2016. Synergistic behavior of betaine-urea mixture: Formation of deep eutectic solvent. *J. Mol. Liq.* 219:74–78.
22. Park, K., B. Y. Ham, …, J. Lee. 2022. Insights into the enhanced thermal stability of lysozyme with altered structure and activity induced by choline chloride-based deep eutectic solvents containing polyols and sugars. *J. Mol. Liq.* 349:118143.
23. Cao, J., R. Wu, …, E. Su. 2022. Enzymes in nearly anhydrous deep eutectic solvents: Insight into the biocompatibility and thermal stability. *Enzym. Microb. Technol.* 157:110022.
24. Mamashli, F., J. Badraghi, …, A. A. Saboury. 2018. Improvement of versatile peroxidase activity and stability by a cholinium-based ionic liquid. *J. Mol. Liq.* 272:597–608.
25. Pal, S., R. Roy, and S. Paul. 2020. Potential of a Natural Deep Eutectic Solvent, Glyceline, in the Thermal Stability of the Trp-Cage Miniprotein. *J. Phys. Chem. B.* 124:7598–7610.
26. Olivares, B., F. Martínez, …, P. R. Campodonico. 2018. A Natural Deep Eutectic Solvent Formulated to Stabilize β-Lactam Antibiotics. *Sci. Rep.* 8:1–12.
27. Gomes, I., and N. Galamba. 2023. Protein stability in a natural deep eutectic solvent: Preferential hydration or solvent slaving? *J. Chem. Phys.* 159:235101.
28. Sanchez-Fernandez, A., J.-F. Poon, …, C. Dicko. 2024. Stabilization of Non-Native Folds and Programmable Protein Gelation in Compositionally Designed Deep Eutectic Solvents. *ACS Nano.* 18:18314–18326.
29. Sun, H., R. Xin, …, F. Yao. 2020. Mechanism of deep eutectic solvents enhancing catalytic function of cytochrome P450 enzymes in biosynthesis and organic synthesis. *J. Biotechnol.* 323:264–273.
30. Das, N., T. Khan, …, P. Sen. 2021. Correlating Bromelain's activity with its structure and active-site dynamics and the medium's physical properties in a hydrated deep eutectic solvent. *Phys. Chem. Chem. Phys.* 23:9337–9346.
31. Esquembre, R., J. M. Sanz, …, M. L. Ferrer. 2013. Thermal unfolding and refolding of lysozyme in deep eutectic solvents and their aqueous dilutions. *Phys. Chem. Chem. Phys.* 15:11248–11256.
32. Kumari, P., M. Kumari, and H. K. Kashyap. 2020. How Pure and Hydrated Reline Deep Eutectic Solvents Affect the Conformation and Stability of Lysozyme: Insights from Atomistic Molecular Dynamics Simulations. *J. Phys. Chem. B.* 124:11919–11927.
33. Dhiman, D., A. S. C. Marques, …, P. Venkatesu. 2023. Unveiling the potential of deep eutectic solvents to improve the conformational and colloidal stability of immunoglobulin G antibodies. *Green Chem.* 25:650–660.
34. Yadav, N., K. Bhakuni, …, P. Venkatesu. 2020. Expanding the Potential Role of Deep Eutectic Solvents toward Facilitating the Structural and Thermal Stability of α-Chymotrypsin. *ACS Sustain. Chem. Eng.* 8:10151–10160.
35. Papadopoulou, A. A., E. Efstathiadou, …, H. Stamatis. 2016. Deep Eutectic Solvents as Media for Peroxidation Reactions Catalyzed by Heme-Dependent Biocatalysts. *Ind. Eng. Chem. Res.* 55:5145–5151.
36. Khan, T., N. Das, …, P. Sen. 2025. Critical Role of Water beyond the Media to Maintain Protein Stability and Activity in Hydrated Deep Eutectic Solvent. *J. Phys. Chem. B.* 129:162–175.
37. Khan, T., N. Das, …, P. Sen. 2023. Understanding the intricacy of protein in hydrated deep eutectic solvent: Solvation dynamics, conformational fluctuation dynamics, and stability. *Int. J. Biol. Macromol.* 253:127100.
38. Sanchez-Fernandez, A., K. J. Edler, …, A. J. Jackson. 2017. Protein conformation in pure and hydrated deep eutectic solvents. *Phys. Chem. Chem. Phys.* 19:8667–8670.
39. Durand, E., J. Lecomte, …, P. Villeneuve. 2014. Towards a better understanding of how to improve lipase-catalyzed reactions using deep eutectic solvents based on choline chloride. *Eur. J. Lipid Sci. Technol.* 116:16–23.
40. Durand, E., J. Lecomte, …, P. Villeneuve. 2013. Evaluation of deep eutectic solvent-water binary mixtures for lipase-catalyzed lipophilization of phenolic acids. *Green Chem.* 15:2275–2282.

41. Choi, Y. H., J. van Spronsen, …, R. Verpoorte. 2011. Are natural deep eutectic solvents the missing link in understanding cellular metabolism and physiology? *Plant Physiol.* 156:1701–1705.

42. Wang, X., Y. Sheng, …, H. Huang. 2024. Corner Engineering: Tailoring Enzymes for Enhanced Resistance and Thermostability in Deep Eutectic Solvents. *Angew. Chem. Int. Ed.* 63:e202315125.

43. Soltani-Nezhad, Z., M. Zaboli, M. Torkzadeh-Mahani…, 2025. Enhancing stability and catalytic activity of urate oxidase using natural deep eutectic solvent: insights from experimental and computational approaches. *J. Biomol. Struct. Dyn.* https://doi.org/10.1080/07391102.2025.2486444.

44. Sanchez-Fernandez, A., M. Basic, …, C. Dicko. 2022. Hydration in Deep Eutectic Solvents Induces Non-monotonic Changes in the Conformation and Stability of Proteins. *J. Am. Chem. Soc.* 144:23657–23667.

45. Bhattacharyya, K. 2008. Nature of biological water: a femtosecond study. *Chem. Commun.* 2008:2848.

46. Bagchi, B. 2005. Water dynamics in the hydration layer around proteins and micelles. *Chem. Rev.* 105:3197–3219.

47. Bellissent-Funel, M. C., A. Hassanali, …, A. E. Garcia. 2016. Water Determines the Structure and Dynamics of Proteins. *Chem. Rev.* 116:7673–7697.

48. Ball, P. 2008. Water as an active constituent in cell biology. *Chem. Rev.* 108:74–108.

49. Khan, T., B. Halder, …, P. Sen. 2024. Role of Associated Water Dynamics on Protein Stability and Activity in Crowded Milieu. *J. Phys. Chem. B.* 128:8672–8686.

50. Das, N., E. Tarif, …, P. Sen. 2023. Associated Water Dynamics Might Be a Key Factor Affecting Protein Stability in the Crowded Milieu. *J. Phys. Chem. B.* 127:3151–3163.

51. Negi, K. S., N. Das, …, P. Sen. 2023. Osmolyte induced protein stabilization: modulation of associated water dynamics might be a key factor. *Phys. Chem. Chem. Phys.* 25:32602–32612.

52. More, S. R., and S. K. Jha. 2025. Multi-Site Red-Edge Excitation Shift Reveals the Residue-Specific Solvation Dynamics during the Native to Amyloid-like Transition of an Amyloidogenic Protein. *J. Phys. Chem. B.* 129:176–193.

53. Raghuraman, H., S. M. Islam, …, E. Perozo. 2014. Dynamics transitions at the outer vestibule of the KcsA potassium channel during gating. *Proc. Natl. Acad. Sci. USA.* 111:1831–1836.

54. Brahma, R., and H. Raghuraman. 2021. Novel insights in linking solvent relaxation dynamics and protein conformations utilizing red edge excitation shift approach. *Emerg. Top. Life Sci.* 5:89–101.

55. Chattopadhyay, A., and S. Haldar. 2014. Dynamic insight into protein structure utilizing red edge excitation shift. *Acc. Chem. Res.* 47:12–19.

56. Das, N., S. Sahu, …, P. Sen. 2023. Site-specific Heterogeneity of Multi-domain Human Serum Albumin and its Origin: A Red Edge Excitation Shift Study. *Photochem. Photobiol.* 99:538–546.

57. Sengupta, B., A. Acharyya, and P. Sen. 2016. Elucidation of the local dynamics of domain-III of human serum albumin over the ps–μs time regime using a new fluorescent label. *Phys. Chem. Chem. Phys.* 18:28548–28555.

58. Yadav, R., B. Sengupta, and P. Sen. 2014. Conformational fluctuation dynamics of domain i of human serum albumin in the course of chemically and thermally induced unfolding using fluorescence correlation spectroscopy. *J. Phys. Chem. B.* 118:5428–5438.

59. Das, N., and P. Sen. 2022. Macromolecular crowding: how shape and interaction affect the structure, function, conformational dynamics and relative domain movement of a multi-domain protein. *Phys. Chem. Chem. Phys.* 24:14242–14256.

60. Sanchez-Fernandez, A., S. Prevost, and M. Wahlgren. 2022. Deep eutectic solvents for the preservation of concentrated proteins: the case of lysozyme in 1 : 2 choline chloride : glycerol. *Green Chem.* 24:4437–4442.

61. Wang, Y., C. Ma, …, X. Ji. 2020. Thermodynamic Study of Choline Chloride-Based Deep Eutectic Solvents with Water and Methanol. *J. Chem. Eng. Data.* 65:2446–2457.

62. Das, N., and P. Sen. 2020. Shape-Dependent Macromolecular Crowding on the Thermodynamics and Microsecond Conformational Dynamics of Protein Unfolding Revealed at the Single-Molecule Level. *J. Phys. Chem. B.* 124:5858–5871.

63. Shil, S., N. Das, …, P. Sen. 2018. Sucrose-Induced Stabilization of Domain-II and Overall Human Serum Albumin against Chemical and Thermal Denaturation. *ACS Omega.* 3:16633–16642.

64. Das, N., and P. Sen. 2019. Size-dependent macromolecular crowding effect on the thermodynamics of protein unfolding revealed at the single molecular level. *Int. J. Biol. Macromol.* 141:843–854.

65. Mohan, G., S. Kuma, …, C. S. Reddy. 2020. Excellency of pyrimidinyl moieties containing α-aminophosphonates over benzthiazolyl moieties for thermal and structural stability of stem bromelain. *Int. J. Biol. Macromol.* 165:2010–2021.

66. Khan, T., E. Tarif, …, P. Sen. 2023. Multiple evidences for molecular level heterogeneity in a non-ionic biocatalytic deep eutectic solvent. *J. Mol. Liq.* 389:122882.

67. Negi, K. S., S. Rana, …, P. Sen. 2025. Interplay of Protein Fluctuation and Associated Water Dynamics in Osmolyte Induced Stabilization. *Biophys. J.* 124:2082–2091.

68. Müller, C. B., A. Loman, …, J. Enderlein. 2008. Precise measurement of diffusion by multi-color dual-focus fluorescence correlation spectroscopy. *Europhys. Lett.* 83:46001.

69. Chung, S., E. Lerner, …, S. Weiss. 2019. The effect of macromolecular crowding on RNA polymerase. *Nucleic Acids Res.* 47:1440–1450.

70. Chakravorty, P., and A. B. Das. 2025. Impact of choline choride and sugar natural deep eutectic solvents on structure and functionality of treebean (Parkia timoriana) seed protein. *Sci. Rep.* 15:3701–3710.

71. Zhou, P., X. Wang, …, Y. Wang. 2017. Chemoenzymatic epoxidation of alkenes with Candida antarctica lipase B and hydrogen peroxide in deep eutectic solvents. *RSC Adv.* 7:12518–12523.

72. Murakami, S., and M. Kinoshita. 2016. Effects of monohydric alcohols and polyols on the thermal stability of a protein. *J. Chem. Phys.* 144:125105.

73. Sukenik, S., L. Sapir, and D. Harries. 2013. Balance of enthalpy and entropy in depletion forces. *Curr. Opin. Colloid Interface Sci.* 18:495–501.

74. Sukenik, S., L. Sapir, …, D. Harries. 2013. Diversity in the mechanisms of cosolute action on biomolecular processes. *Faraday Discuss.* 160:225–327.

75. Denisov, V. P., B. H. Jonsson, and B. Halle. 1999. Hydration of denatured and molten globule proteins. *Nat. Struct. Biol.* 6:253–260.

76. Li, C., and M. Liu. 2013. Protein dynamics in living cells studied by in-cell NMR spectroscopy. *FEBS Lett.* 587:1008–1011.

77. Svergun, D. I., S. Richard, …, G. Zaccai. 1998. Protein hydration in solution: Experimental observation by x-ray and neutron scattering. *Proc. Natl. Acad. Sci. USA.* 95:2267–2272.

78. Gerstein, M., and C. Chothia. 1996. Packing at the protein-water interface. *Proc. Natl. Acad. Sci. USA.* 93:10167–10172.

79. Burling, F. T., W. I. Weis, …, A. T. Brünger. 1996. Direct observation of protein solvation and discrete disorder with experimental crystallographic phases. *Science.* 271:72–77.

80. Smith, L. J., A. M. Bowen, …, C. Redfield. 2013. The dynamics of lysozyme from bacteriophage lambda in solution probed by NMR and MD simulations. *Chembiochem.* 14:1780–1788.

81. Marlow, M. S., J. Dogan, …, A. J. Wand. 2010. The role of conformational entropy in molecular recognition by calmodulin. *Nat. Chem. Biol.* 6:352–358.

82. Frederick, K. K., M. S. Marlow, …, A. J. Wand. 2007. Conformational entropy in molecular recognition by proteins. *Nature.* 448:325–329.

83. Nandi, N., and B. Bagchi. 1997. Dielectric Relaxation of Biological Water. *J. Phys. Chem. B.* 101:10954–10961.

84. Nandi, N., K. Bhattacharyya, and B. Bagchi. 2000. Dielectric relaxation and solvation dynamics of water in complex chemical and biological systems. *Chem. Rev.* 100:2013–2046.
85. Russo, D., R. K. Murarka, …, T. Head-Gordon. 2005. Molecular view of water dynamics near model peptides. *J. Phys. Chem. B.* 109:12966–12975.
86. Lorenz-Ochoa, K. A., and C. R. Baiz. 2023. Ultrafast Spectroscopy Reveals Slow Water Dynamics in Biocondensates. *J. Am. Chem. Soc.* 145:27800–27809.
87. Laage, D., T. Elsaesser, and J. T. Hynes. 2017. Water Dynamics in the Hydration Shells of Biomolecules. *Chem. Rev.* 117:10694–10725.
88. Dopfer, O., and M. Fujii. 2016. Probing Solvation Dynamics around Aromatic and Biological Molecules at the Single-Molecular Level. *Chem. Rev.* 116:5432–5463.
89. Pignataro, M. F., M. G. Herrera, and V. I. Dodero. 2020. Evaluation of Peptide/Protein Self-Assembly and Aggregation by Spectroscopic Methods. *Molecules.* 25:4854.
90. Fogarty, A. C., E. Duboué-Dijon, …, D. Laage. 2013. Biomolecular hydration dynamics: a jump model perspective. *Chem. Soc. Rev.* 42:5672–5683.
91. Levy, Y., and J. N. Onuchic. 2006. Water Mediation in Protein Folding and Molecular Recognition. *Annu. Rev. Biophys. Biomol. Struct.* 35:389–415.
92. Leitner, D. M., M. Gruebele, and M. Havenith. 2008. Solvation dynamics of biomolecules: Modeling and terahertz experiments. *HFSP J.* 2:314–323.
93. Chattopadhyay, A. 2003. Exploring membrane organization and dynamics by the wavelength-selective fluorescence approach. *Chem. Phys. Lipids.* 122:3–17.
94. Mishra, P., and S. K. Jha. 2019. Slow Motion Protein Dance Visualized Using Red-Edge Excitation Shift of a Buried Fluorophore. *J. Phys. Chem. B.* 123:1256–1264.
95. Demchenko, A. P. 2002. The red-edge effects: 30 years of exploration. *Luminescence.* 17:19–42.
96. Demchenko, A. P. 1985. Fluorescence molecular relaxation studies of protein dynamics: The probe binding site of melittin is rigid on the nanosecond time scale. *FEBS Lett.* 182:99–102.
97. Demchenko, A. P. 1982. On the nanosecond mobility in proteins: Edge excitation fluorescence red shift of protein-bound 2-(p-toluidinylnaphthalene)-6-sulfonate. *Biophys. Chem.* 15:101–109.
98. Demchenko, A. P. 2016. Weber's Red-Edge Effect that Changed the Paradigm in Photophysics and Photochemistry. Perspectives on Fluorescence, Springer Series on Fluorescence. *Springer.* 17:95–141.
99. Das, N., T. Khan, and P. Sen. 2024. The shift of excitation spectra at blue edge of emission (BEEmS) as a new methodology to probe heterogeneity. *Chem. Phys.* 577:112138.
100. Chen, G., Q. Zhang, …, B. Feng. 2019. Protection effect of polyols on Rhizopus chinensis lipase counteracting the deactivation from high pressure and high temperature treatment. *Int. J. Biol. Macromol.* 127:555–562.
101. Rao, C. M., S. C. Rao, and P. B. Rao. 1989. Red edge excitation effect in intact eye lens. *Photochem. Photobiol.* 50:399–402.
102. Rao, S. C., and C. M. Rao. 1994. Red edge excitation shifts of crystallins and intact lenses: A study of segmental mobility and inter-protein interactions. *FEBS Lett.* 337:269–273.
103. Muthu, S. A., H. C. Jadav, …, B. Ahmad. 2020. The reorganization of conformations, stability and aggregation of serum albumin isomers through the interaction of glycopeptide antibiotic teicoplanin: A thermodynamic and spectroscopy study. *Int. J. Biol. Macromol.* 163:66–78.
104. Patra, S. K., and M. K. Pal. 1997. Red edge excitation shift emission spectroscopic investigation of serum albumins and serum albumin-bilirubin complexes. *Spectrochim. Acta, Part A.* 53A:1609–1614.
105. Batey, S., and J. Clarke. 2008. The Folding Pathway of a Single Domain in a Multidomain Protein is not Affected by Its Neighbouring Domain. *J. Mol. Biol.* 378:297–301.
106. Santorelli, D., L. Marcocci, …, S. Gianni. 2023. Understanding the molecular basis of folding cooperativity through a comparative analysis of a multidomain protein and its isolated domains. *J. Biol. Chem.* 299:102983.
107. Varshney, A., B. Ahmad, and R. H. Khan. 2008. Comparative studies of unfolding and binding of ligands to human serum albumin in the presence of fatty acid: Spectroscopic approach. *Int. J. Biol. Macromol.* 42:483–490.
108. Muzammil, S., Y. Kumar, and S. Tayyab. 2000. Anion-induced stabilization of human serum albumin prevents the formation of intermediate during urea denaturation. *Proteins.* 40:29–38.
109. Yadav, R., and P. Sen. 2013. Mechanistic investigation of domain specific unfolding of human serum albumin and the effect of sucrose. *Protein Sci.* 22:1571–1581.
110. Mohan, V., B. Sengupta, …, P. Sen. 2018. Region-Specific Double Denaturation of Human Serum Albumin: Combined Effects of Temperature and GnHCl on Structural and Dynamical Responses. *ACS Omega.* 3:10406–10417.
111. Santra, M. K., A. Banerjee, …, D. Panda. 2005. Unfolding pathways of human serum albumin: Evidence for sequential unfolding and folding of its three domains. *Int. J. Biol. Macromol.* 37:200–204.
112. Dockal, M., D. C. Carter, and F. Rüker. 1999. The Three Recombinant Domains of Human Serum Albumin: Structural Characterization and Ligand Binding Properties. *J. Biol. Chem.* 274:29303–29310.
113. Yadav, R., B. Sengupta, and P. Sen. 2016. Effect of sucrose on chemically and thermally induced unfolding of domain-I of human serum albumin: Solvation dynamics and fluorescence anisotropy study. *Biophys. Chem.* 211:59–69.
114. Ahmad, B., M. Z. Ahmed, …, R. H. Khan. 2005. Guanidine hydrochloride denaturation of human serum albumin originates by local unfolding of some stable loops in domain III. *Biochim. Biophys. Acta.* 1750:93–102.
115. Mohan, V., B. Sengupta, …, P. Sen. 2019. Domain-Specific Stabilization of Structural and Dynamic Responses of Human Serum Albumin by Sucrose. *Protein Pept. Lett.* 26:287–300.
116. Senisterra, G., I. Chau, and M. Vedadi. 2012. Thermal denaturation assays in chemical biology. *Assay Drug Dev. Technol.* 10:128–136.
117. Rozas, S., C. Benito, …, S. Aparicio. 2021. Insights on the water effect on deep eutectic solvents properties and structuring: The archetypical case of choline chloride + ethylene glycol. *J. Mol. Liq.* 344:117717.
118. Ferreira, A. S. D., R. Craveiro, …, A. Paiva. 2021. Effect of water on the structure and dynamics of choline chloride/glycerol eutectic systems. *J. Mol. Liq.* 342:117463.
119. Hammond, O. S., D. T. Bowron, and K. J. Edler. 2017. The Effect of Water upon Deep Eutectic Solvent Nanostructure: An Unusual Transition from Ionic Mixture to Aqueous Solution. *Angew. Chem. Int. Ed.* 129:9914–9917.
120. Ma, C., A. Laaksonen, …, X. Ji. 2018. The peculiar effect of water on ionic liquids and deep eutectic solvents. *Chem. Soc. Rev.* 47:8685–8720.

Biophysical Journal, Volume *124*

Supplemental information

Site-specific water dynamics drives protein stability in hydrated deep eutectic solvents

Tanmoy Khan, Kuntal Debnath, Kuldeep Singh Negi, and Pratik Sen

Site-Specific Water Dynamics Drives Protein Stability in Hydrated Deep Eutectic Solvents

Tanmoy Khan, Kuntal Debnath, Kuldeep Singh Negi, and Pratik Sen*

Department of Chemistry, Indian Institute of Technology Kanpur, Kanpur-208016, UP, India

*Corresponding author; Email: psen@iitk.ac.in

Content

Section S1: FCS setup and analysis

We have performed fluorescence correlation spectroscopic (FCS) measurements on an instrument built in our laboratory (1–3). We have used an inverted microscope (IX-71, Olympus, Japan) with a 60X 1.2 NA water-immersion objective (UplanSApo, Olympus, Japan) in this setup. The sample was kept on a cover slip (Blue Star, Polar Industrial Corporation, India) on the microscope sample platform. A 532 nm (MGL-III-532-5mW, DreamLaser, China) laser source was used to create a confocal observation volume. The data has been collected from the 40 μm above the upper surface of the cover slip within the created observation volume. The emitted photons, collected using the same objective, travel through a dichroic mirror (ZT532rdc, Chroma Tech. Corp., USA, for 532 nm excitation), emission filter (605/70m, Chroma Tech. Corp., USA) and divided into two parts using a 50:50 beam splitter and directed to two detectors (SPCM-AQRH-13-FC, Excelitas Tech. Inc., Canada) through multimode fiber patch chord (M67L01 25/50/100 μm 0.10 NA, ThorLabs, USA). The detected photons through two detectors were correlated using a correlator card (FLEX990EM-12E, correlator.com, USA) and displayed using the LabVIEW platform on a computer. Assuming a Gaussian detection volume, for a single-component diffusive system without any additional reaction, the fluorescence intensity correlation function can be written as (4, 5)

$$G(\tau) = \frac{1}{N}\left(1 + \frac{\tau}{\tau_D}\right)^{-1}\left(1 + \frac{\tau}{\omega^2\tau_D}\right)^{-1/2} \quad \text{(S1)}$$

In the above equations, τ_D is the time constant for diffusion, N is the average number of particles in the observation volume, $\omega = \frac{l}{r}$ is the ratio of the longitudinal to transverse radius of the 3D Gaussian volume.

In the presence of a reaction component with time constant τ_R, which contributes to the fluorescence intensity fluctuations in the observation volume in addition to the diffusion, the equation is modified to (4, 5)

$$G(\tau) = \frac{1}{N}\left(1 + \frac{\tau}{\tau_D}\right)^{-1}\left(1 + \frac{\tau}{\omega^2\tau_D}\right)^{-1/2}\left(1 + K\,exp\left(-\frac{\tau}{\tau_R}\right)\right) \quad \text{(S2)}$$

Where, $K = \frac{k_{AB}}{k_{BA}} = \frac{C_B}{C_A}$ is the equilibrium constant for the reaction- $A \rightleftharpoons B$ with forward and backward rate constants of k_{AB} and k_{BA}, respectively.

If the system exhibits singlet-triplet conversion, one more reaction component (τ_T) will add up as (4)

$$G(\tau) = \frac{1}{N}\left(1 + \frac{\tau}{\tau_D}\right)^{-1}\left(1 + \frac{\tau}{\omega^2\tau_D}\right)^{-\frac{1}{2}}\left(1 + K\, exp\left(-\frac{\tau}{\tau_R}\right)\right)\left(1 + \frac{p}{1-p}\, exp\left(-\frac{\tau}{\tau_T}\right)\right) \quad \text{(S3)}$$

where p is the fraction of the dye molecules in the triplet state.

We measured several fluorescence intensity correlation curves of rhodamine 6G ($R6G$) at varying concentrations in water and fitted them globally employing equation 1 to determine the value of ω. While calibrating the value of ω, the diffusion coefficient (D_t) of $R6G$ in water has been taken to be 4.14×10^{-6} cm^2 s^{-1} (6). For a particular set of experiments, while fitting the data with equations 2 or 3, the same value of ω has been used. The value of transverse radius (r) of the observation volume is calculated using

$$r = \sqrt{4\tau_D D_t} \quad \text{(S4)}$$

where, τ_D is the diffusion time and D_t is the diffusion coefficient of the molecule. The observation volume of our FCS setup is estimated to be ~ 0.8 fL (using 50 µm fiber patch chord) using

$$V_{eff} = \pi^{\frac{3}{2}} r^2 l \quad \text{(S5)}$$

In the presence of DES, the refractive index and the viscosity of the solution may change significantly, which need to be corrected to get the diffusion coefficient. The refractive index change is compensated by changing the objective collar position to achieve the lowest diffusion time value for each of the samples (7). In this way, we maintain the lowest detection volume attainable for each sample. We have rectified the effects of viscosity changes through performing control experiments at every experimental point taking $R6G$ as the fluorophore. $R6G$ is a rigid molecule and will not undergo any structural changes when exposed to aqueous

solution of additives. In this way, any changes in its diffusion time through the detection volume will be solely because of differences in the medium viscosity. Using this information and the reported value of the hydrodynamic radius of $R6G$ (7.7 Å) in pH 7.4 buffer, we have calculated the hydrodynamic radius of HSA at every experimental point using the following equation.

$$r_H^{HSA} = r_H^{R6G} \times \frac{\tau_D^{HSA}}{\tau_D^{R6G}} \quad \text{(S6)}$$

As in this case we have used TMR-tagged HSA and TMR is known to have a triplet photophysics in the μs timescale along with the known conformational fluctuation time, we have used the equation 3 (that contains two time constants, τ_R and τ_T, apart from the diffusion time, τ_D) for fitting the autocorrelation curves of protein in the presence of different DES concentrations. For the control experiment, where only rhodamine has been taken, the equation 2 have been used because of the presence of triplet timescale along with diffusion process.

Section S2: Temperature-dependent CD-spectra of HSA in the presence of different concentrations of ChCl-EG and ChCl-Gly DES

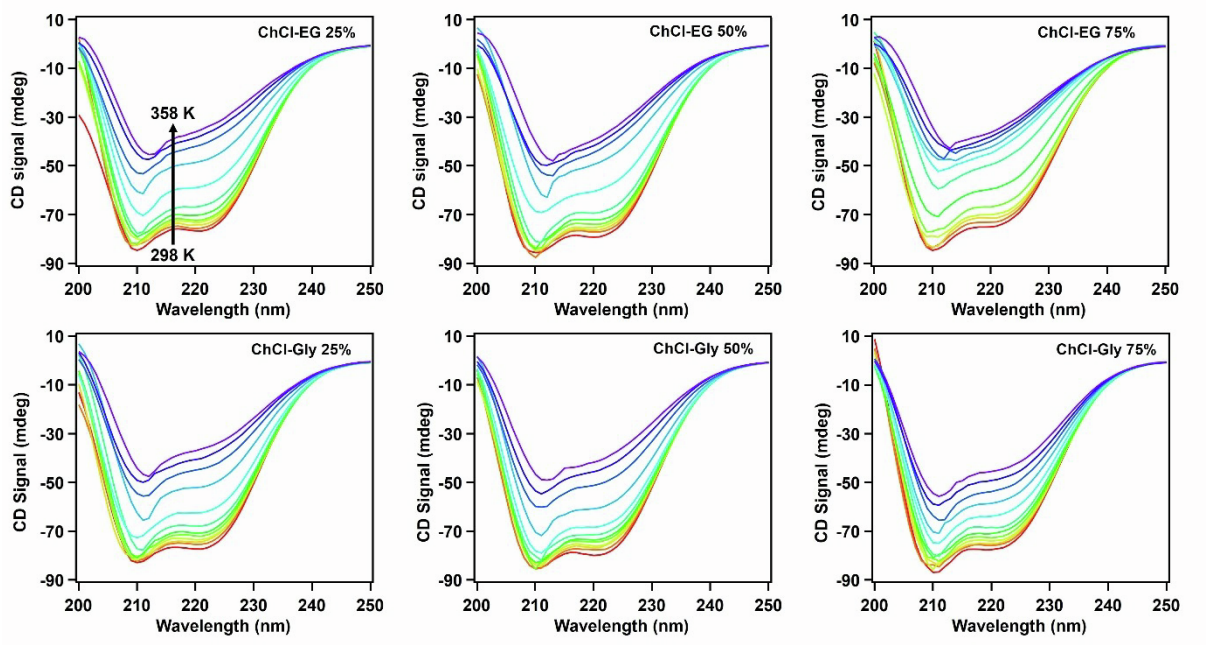

Figure S1. Representative circular dichroism (CD) spectra of HSA in the presence of different concentrations of ChCl-EG and ChCl-Gly DES (the concentrations are mentioned in each figure itself) at different temperatures (298 – 358 K).

Section S3: Excitation wavelength-dependent emission of Domain-I of (CPM-tagged) HSA in the presence of hydrated DESs

In the presence of ChCl-EG DES:

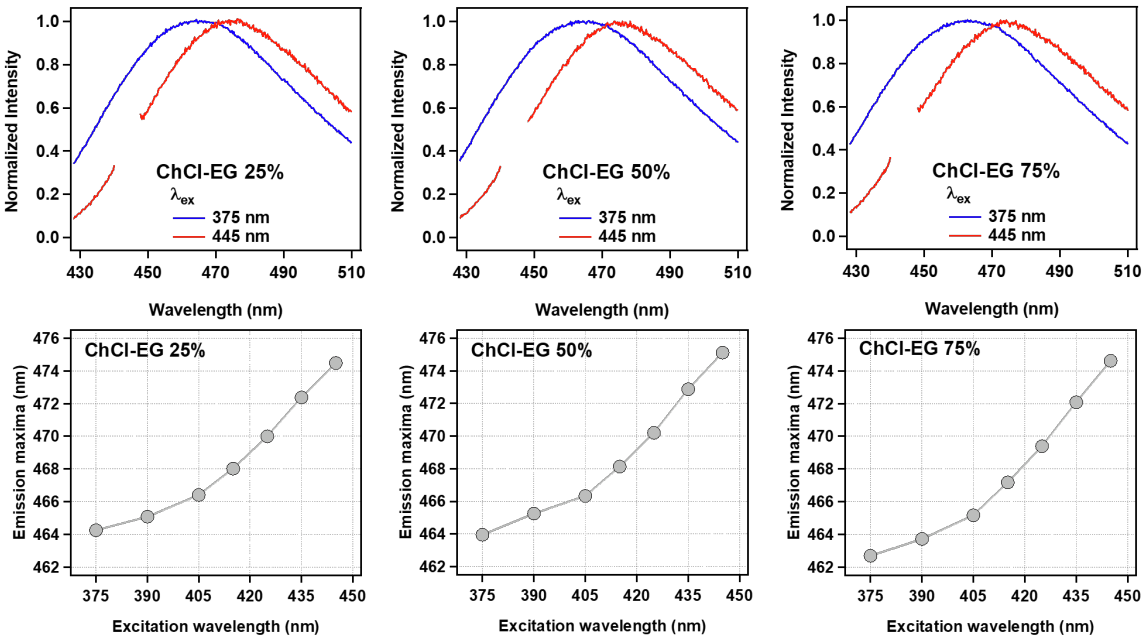

Figure S2. (upper panel) Excitation wavelength-dependent emission spectra of CPM tagged to HSA (domain I); (lower panel) Shift of the emission maxima of CPM tagged to HSA (domain I) with the change in the excitation wavelength in various concentrations of hydrated ChCl-EG DES. The concentrations of the DES are mentioned in each figure itself.

In the presence of ChCl-Gly DES:

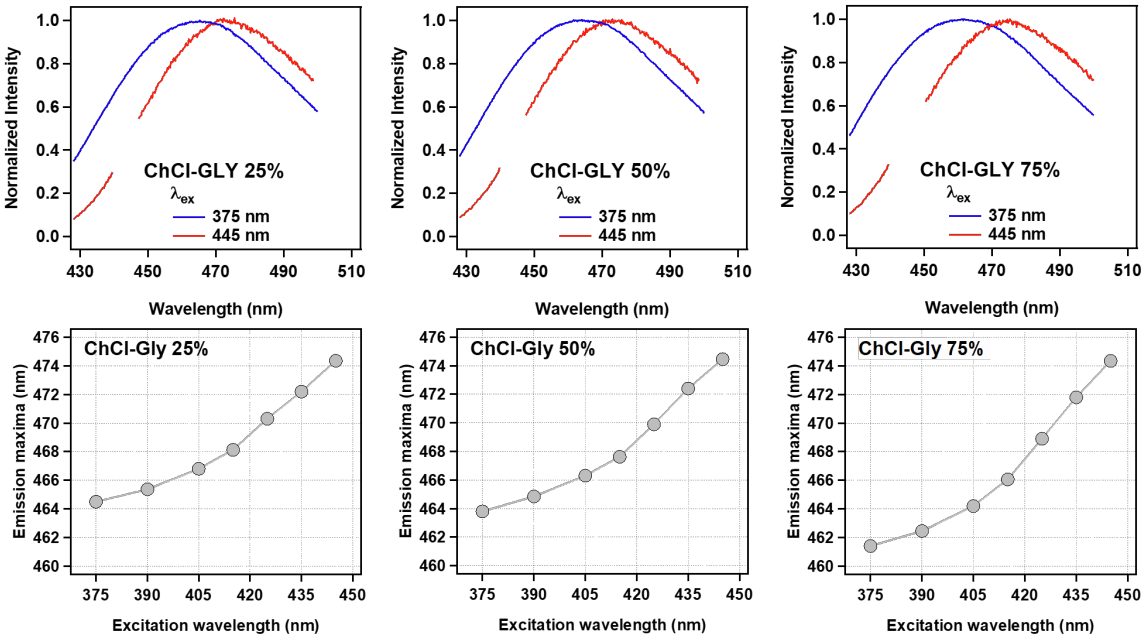

Figure S3. (In the upper panel) Excitation wavelength-dependent emission spectra of CPM tagged to HSA (domain I); (In the lower panel) Shift of the emission maxima of CPM tagged to HSA (domain I) with the change in the excitation wavelength in various concentrations of hydrated ChCl-Gly DES. The concentrations of the DES are mentioned in each figure itself.

Section S4: Excitation wavelength-dependent emission of Domain-III of (NPCE-tagged) HSA in the presence of hydrated DESs

In the presence of ChCl-EG DES:

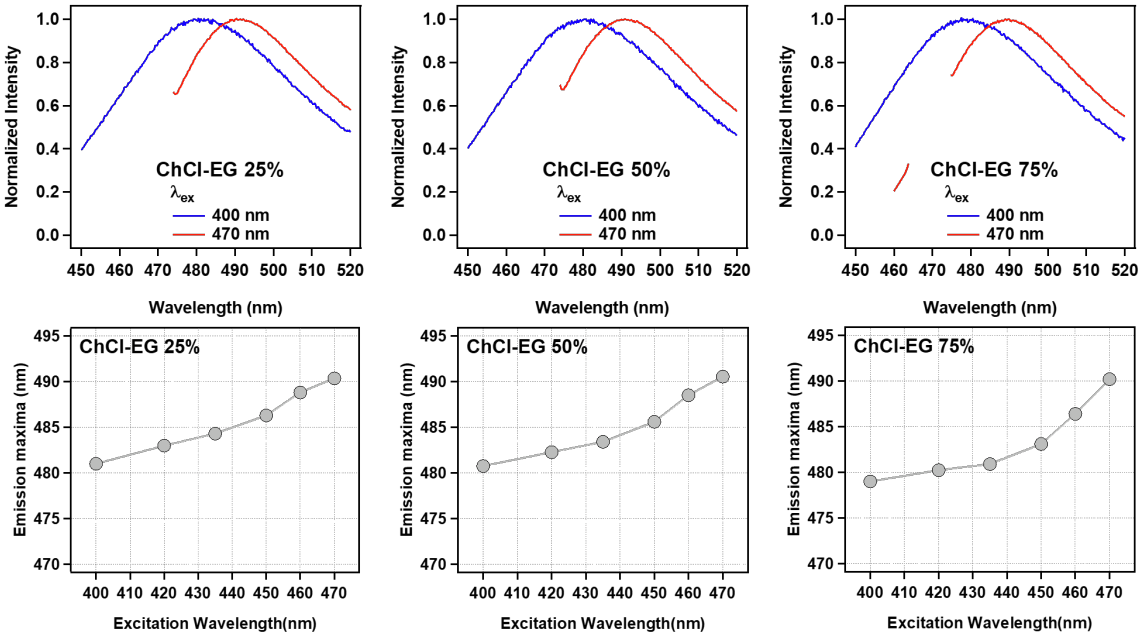

Figure S4. (In the upper panel) Excitation wavelength-dependent emission spectra of NPCE tagged to HSA (domain III); (In the lower panel) Shift of the emission maxima of NPCE tagged to HSA (domain III) with the change in the excitation wavelength in various concentrations of hydrated ChCl-EG DES.

In the presence of ChCl-Gly DES:

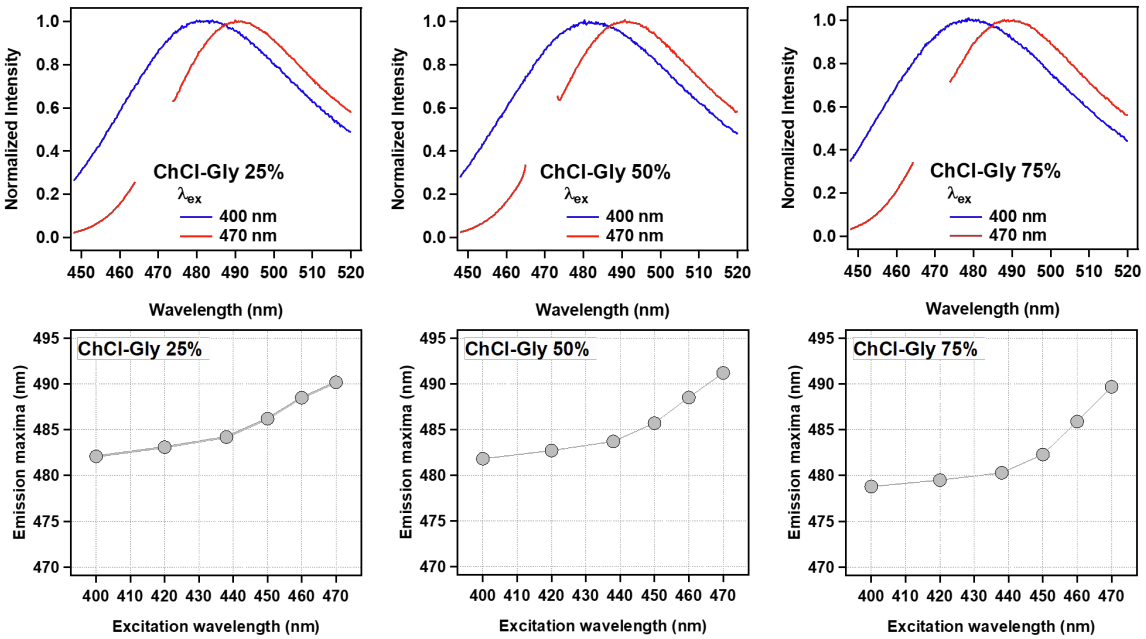

Figure S5. (In the upper panel) Excitation wavelength-dependent emission spectra of NPCE tagged to HSA (domain III); (In the lower panel) Shift of the emission maxima of NPCE tagged to HSA (domain III) with the change in the excitation wavelength in various concentrations of hydrated ChCl-Gly DES.

Section S5: Temperature-dependent steady-state emission study (thermal stability) of HSA domain I and domain III in the presence of different concentrations of hydrated ChCl-EG and ChCl-Gly DESs.

Domain-I:

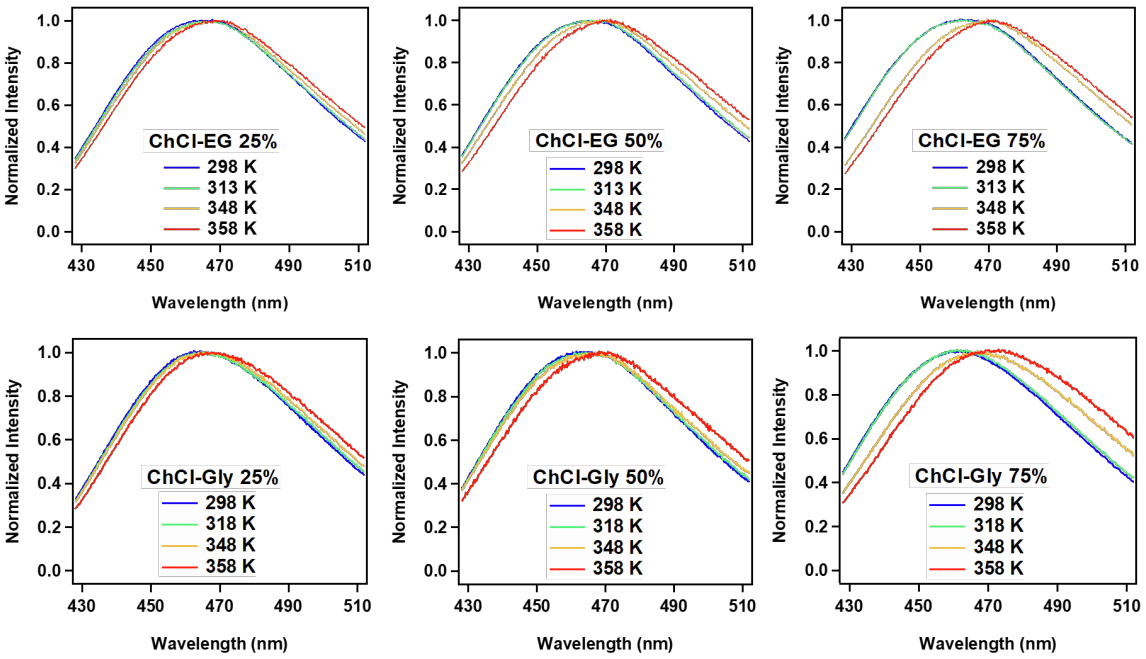

Figure S6. Steady-state fluorescence spectra of CPM-tagged HSA (domain I) at different representative temperatures in the presence of different concentrations of (a) ChCl-EG and (b) ChCl-Gly DES.

Domain-III:

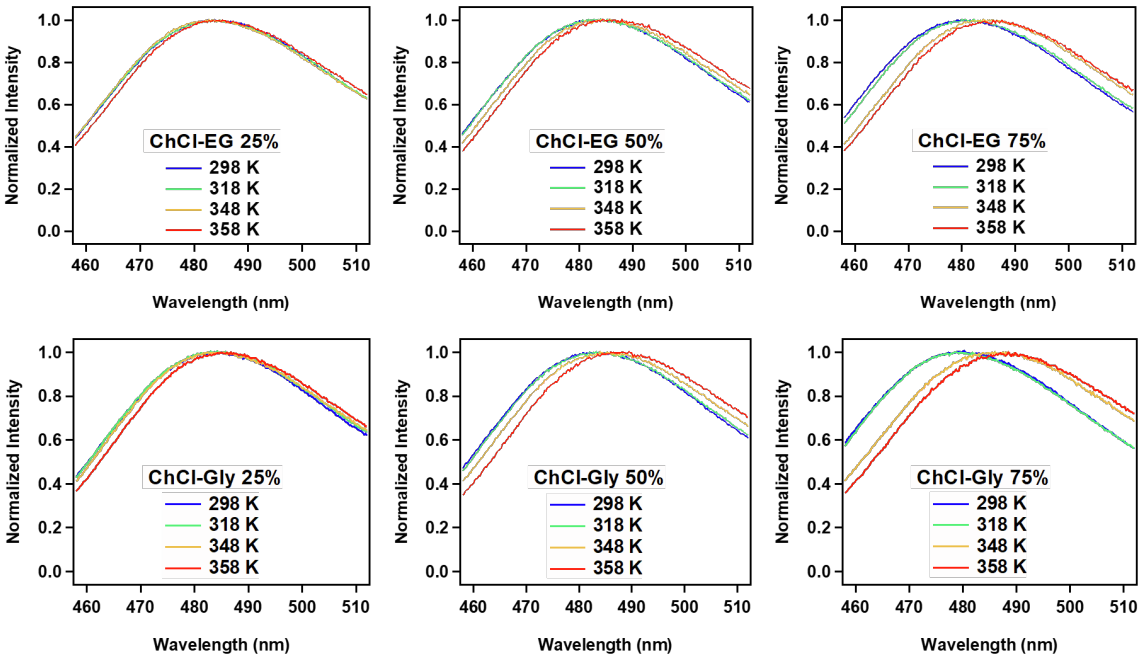

Figure S7. Steady-state fluorescence spectra of NPCE-tagged HSA (domain III) at different representative temperatures in the presence of different concentrations of (a) ChCl-EG and (b) ChCl-Gly DES.

Melting Curves:

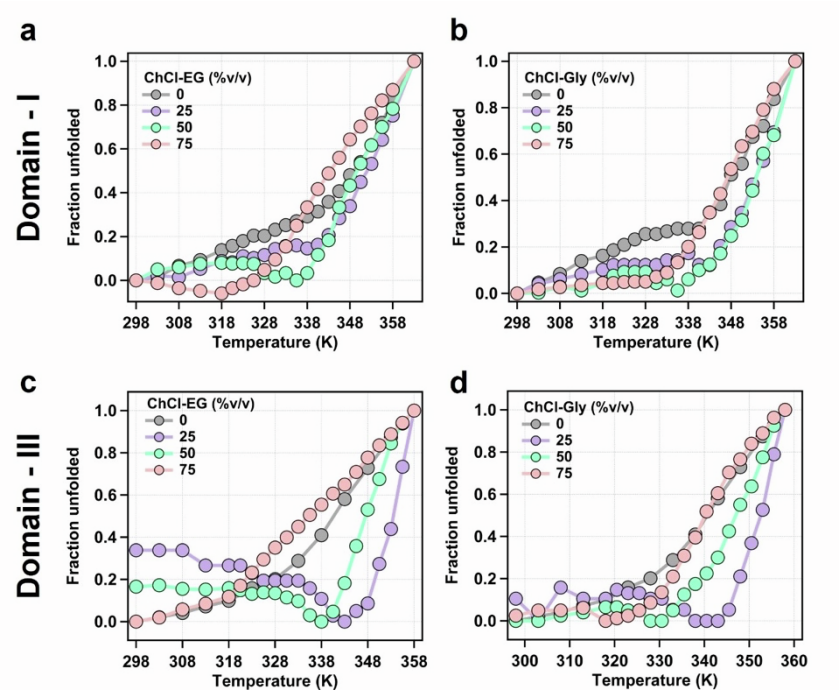

Figure S8. Domain-wise thermal unfolding curve for different concentrations of DESs. The upper panel represents the thermal unfolding curve for CPM-tagged (domain I) HSA in the presence of different concentrations of (a) ChCl-EG and (b) ChCl-Gly DES. The lower panel represents the thermal unfolding curve for NPCE-tagged (domain-III) HSA in the presence of different concentrations of (c) ChCl-EG and (d) ChCl-Gly DES.

Section S6: Fluorescence intensity autocorrelation curves of rhodamine 6G in different concentrations of hydrated ChCl-EG and ChCl-Gly DES and component solution of the same concentration as in hydrated DES.

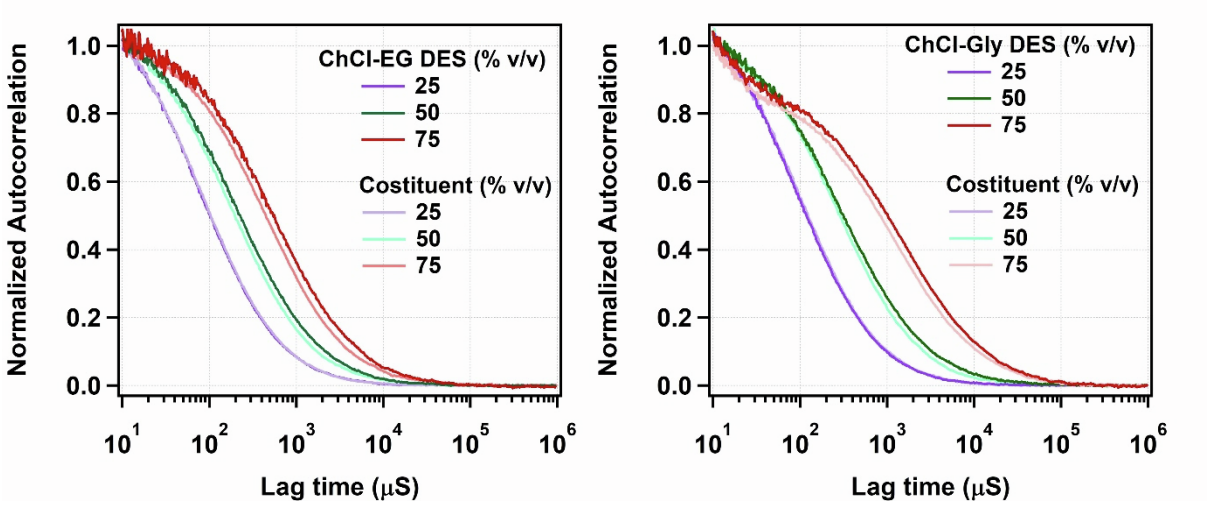

Figure S9. Representative fluorescence intensity autocorrelation curves of R6G in hydrated DES and component solution of the same concentration as in hydrated DES. The concentrations of the constituents are mentioned in each figure itself.

Section S7: Temperature-dependent CD-spectra of HSA in the presence of different concentrations of ChCl, ethylene glycol, and glycerol.

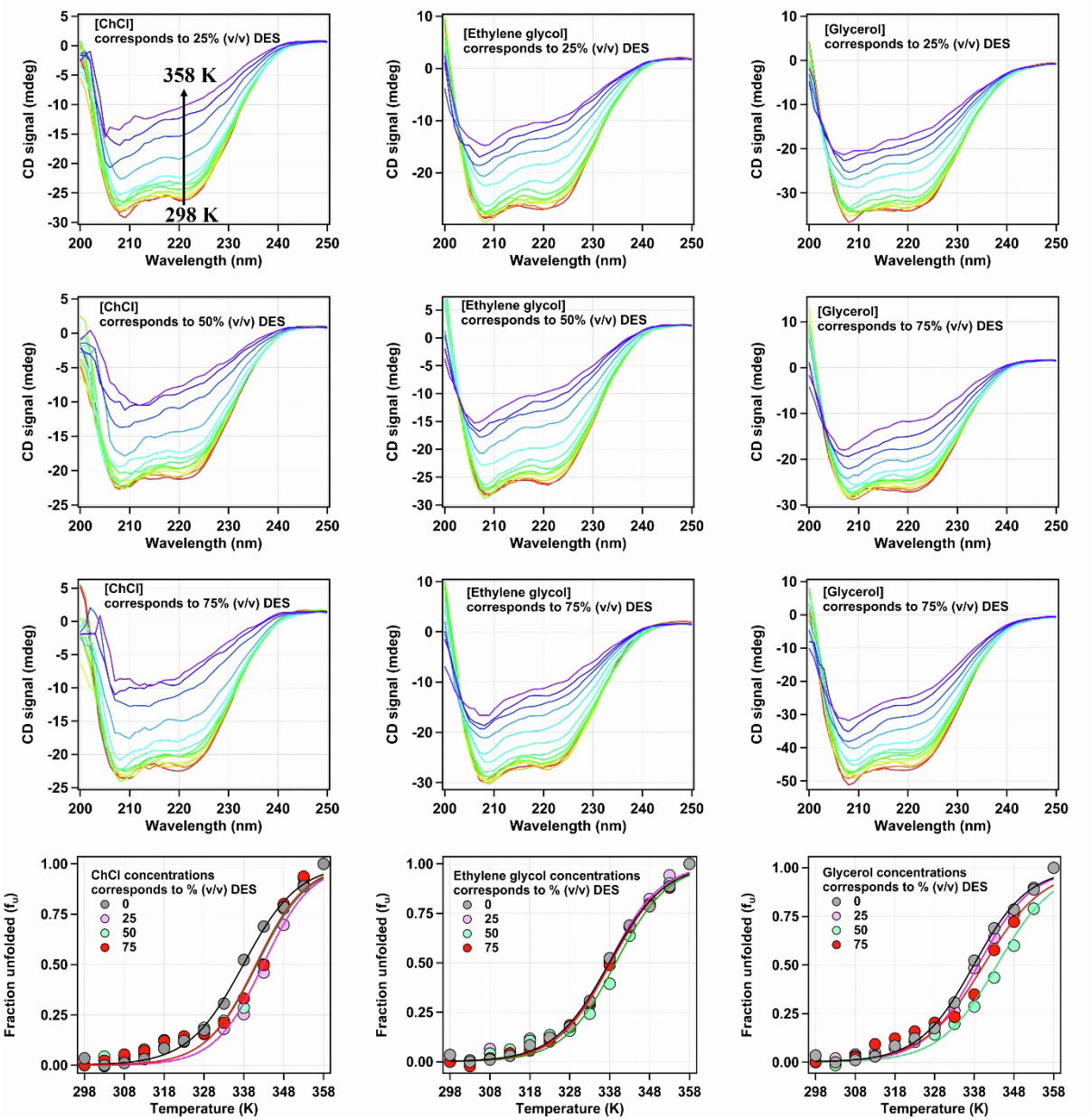

Figure S10. Representative circular dichroism (CD) spectra of HSA in the presence of different concentrations of ChCl (left panel), EG (middle panel), and glycerol (right panel) at different temperatures (298 – 358 K). The concentrations are mentioned in each figure itself. The lowermost row represents the melting curves of the HSA thermal unfolding in the presence of ChCl, ethylene glycol, and glycerol, respectively, from left to right at different concentrations as mentioned in the figure legend itself.

Section S8: Excitation wavelength-dependent emission of Domain-I of (CPM-tagged) HSA in the presence of different concentrations of ChCl, ethylene glycol, and glycerol.

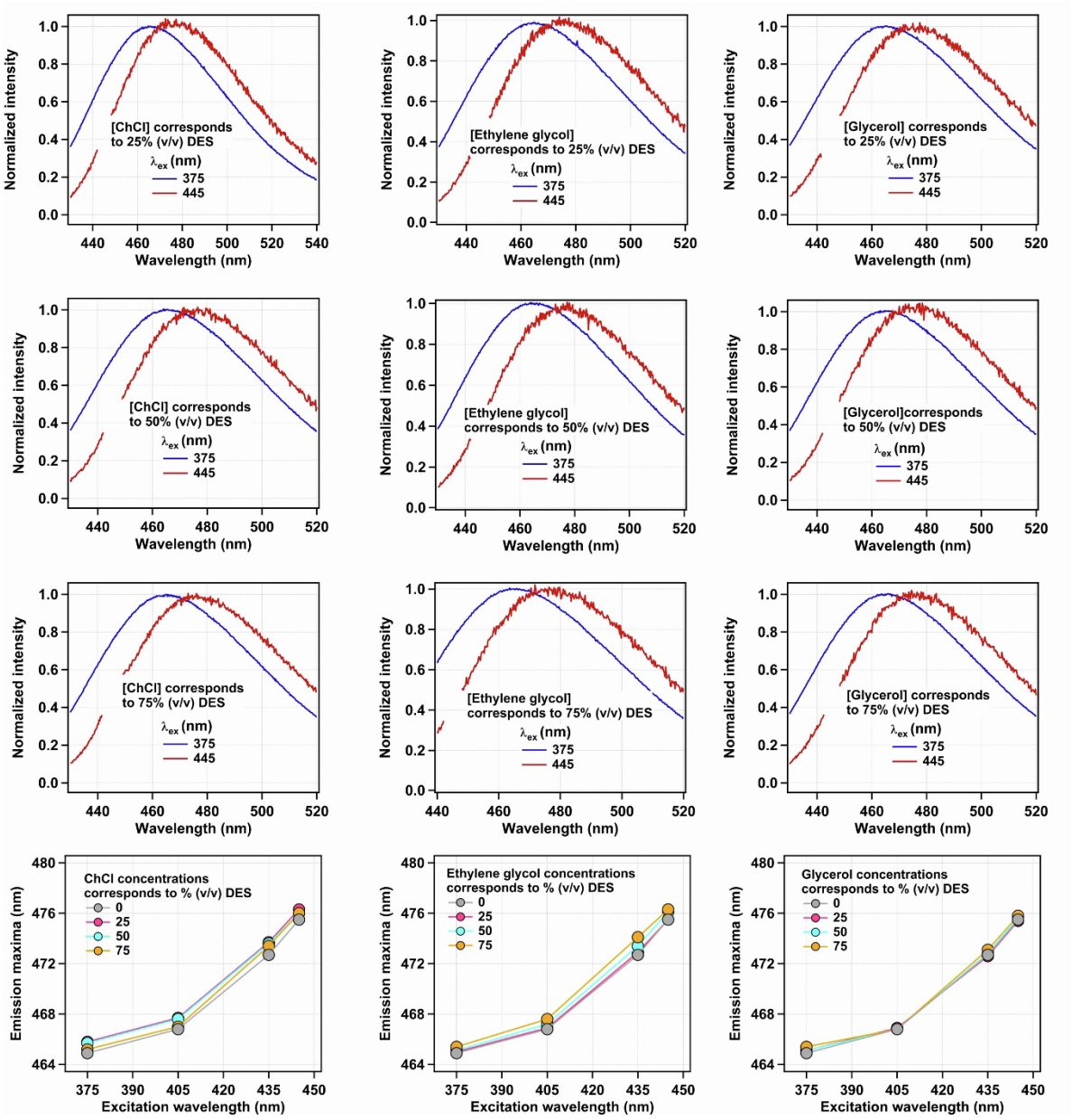

Figure S11. (In the upper panel) Excitation wavelength-dependent emission spectra of CPM tagged to HSA (domain I); (In the lowermost panel) Shift of the emission maxima of CPM tagged to HSA (domain I) with the change in the excitation wavelength in various concentrations of ChCl, Ethylene glycol, and Glycerol. The concentrations of the constituents are mentioned in each figure itself.

Section S9: Excitation wavelength-dependent emission of Domain-III of (NPCE-tagged) HSA in the presence of different concentrations of ChCl, ethylene glycol, and glycerol.

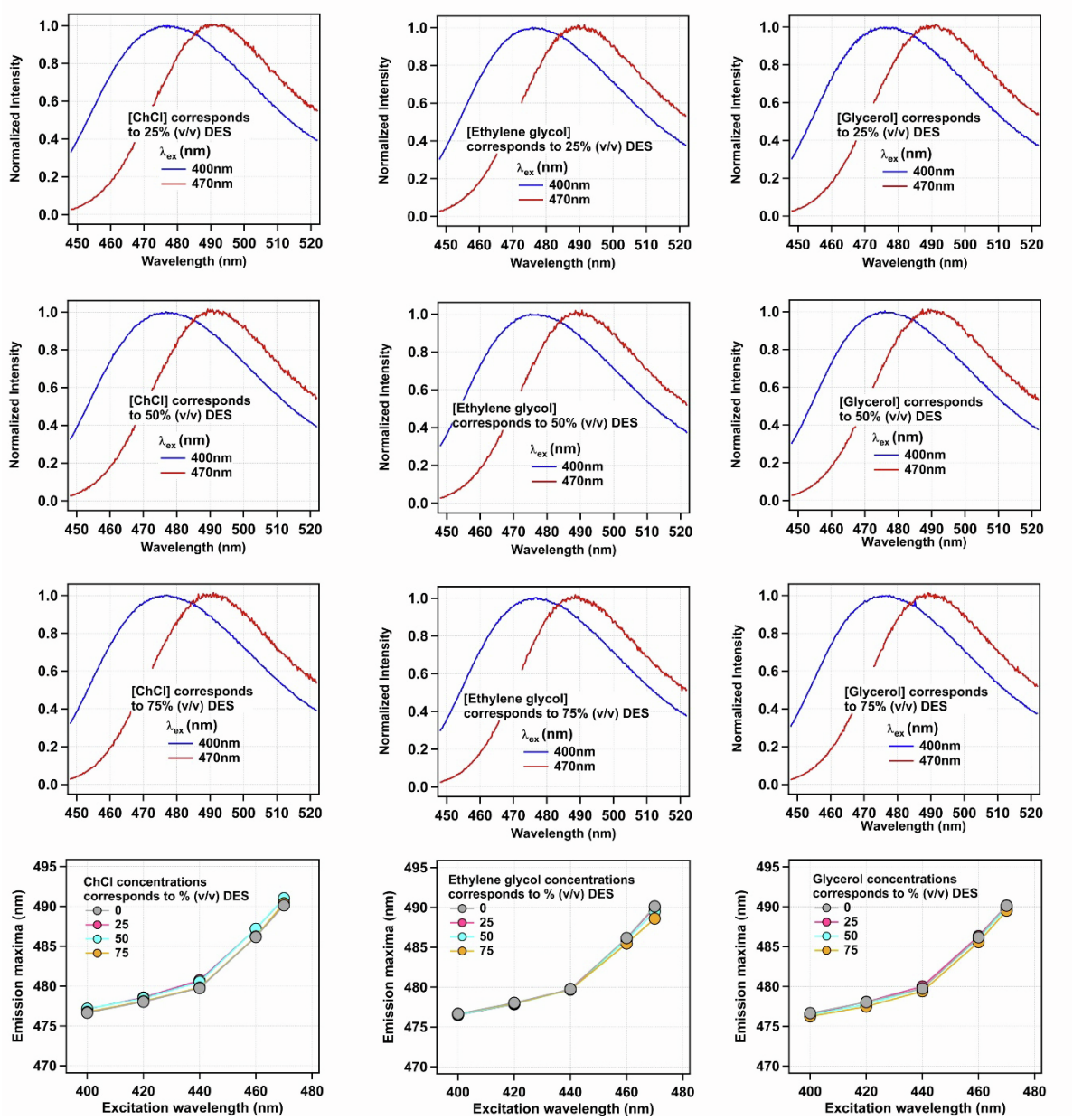

Figure S12. Excitation wavelength-dependent emission spectra of NPCE tagged to HSA (domain III); and the shift of the emission maxima of NPCE tagged to HSA (domain I) with the change in the excitation wavelength in various concentrations of ChCl (left panel), Ethylene glycol (middle panel), and Glycerol (right panel). The concentrations of the constituents are mentioned in each figure itself.

References:

S1. Das, N., T. Khan, N. Subba, and P. Sen. 2021. Correlating Bromelain's activity with its structure and active-site dynamics and the medium's physical properties in a hydrated deep eutectic solvent. *Phys. Chem. Chem. Phys*. 23:9337–9346.

S2. Khan, T., E. Tarif, Y. Awano, L.S. Lozada, N. Das, K. Tominaga, and P. Sen. 2023. Multiple evidences for molecular level heterogeneity in a non-ionic biocatalytic deep eutectic solvent. *J. Mol. Liq.* 389:122882.

S3. Das, N., and P. Sen. 2020. Shape-Dependent Macromolecular Crowding on the Thermodynamics and Microsecond Conformational Dynamics of Protein Unfolding Revealed at the Single-Molecule Level. *J. Phys. Chem. B*. 124:5858–5871.

S4. Krichevsky, O., and G. Bonnet. 2002. Fluorescence correlation spectroscopy: the technique and its applications. *Rep. Prog. Phys.* 65:251–297.

S5. Wohland, T., S. Maiti, and R. Macháň. 2020. An Introduction to Fluorescence Correlation Spectroscopy. IOP Publishing.

S6. Müller, C.B., A. Loman, V. Pacheco, F. Koberling, D. Willbold, W. Richtering, and J. Enderlein. 2008. Precise measurement of diffusion by multi-color dual-focus fluorescence correlation spectroscopy. *Epl*. 83:1–5.

S7. Pal, N., S.D. Verma, M.K. Singh, and S. Sen. 2011. Fluorescence correlation spectroscopy: An efficient tool for measuring size, size-distribution and polydispersity of microemulsion droplets in solution. *Anal. Chem.* 83:7736–7744.